Published in final edited form as:

Cell Rep. 2023 July 25; 42(7): 112694. doi:10.1016/j.celrep.2023.112694.

Structures of 9-1-1 DNA checkpoint clamp loading at gaps from start to finish and ramification on biology

Fengwei Zheng[1], **Roxana E. Georgescu**[2], **Nina Y. Yao**[2], **Michael E. O'Donnell**[2,3,*], **Huilin Li**[1,4,*]

[1]Department of Structural Biology, Van Andel Institute, Grand Rapids, MI, USA

[2]DNA Replication Laboratory, The Rockefeller University, New York, NY, USA

[3]Howard Hughes Medical Institute, The Rockefeller University, New York, NY, USA

[4]Lead contact

SUMMARY

Rad24-RFC (replication factor C) loads the 9-1-1 checkpoint clamp onto the recessed 5′ ends by binding a 5′ DNA at an external surface site and threading the 3′ single-stranded DNA (ssDNA) into 9-1-1. We find here that Rad24-RFC loads 9-1-1 onto DNA gaps in preference to a recessed 5′ end, thus presumably leaving 9-1-1 on duplex 3′ ss/double-stranded DNA (dsDNA) after Rad24-RFC ejects from DNA. We captured five Rad24-RFC-9-1-1 loading intermediates using a 10-nt gap DNA. We also determined the structure of Rad24-RFC–9-1-1 using a 5-nt gap DNA. The structures reveal that Rad24-RFC is unable to melt DNA ends and that a Rad24 loop limits the dsDNA length in the chamber. These observations explain Rad24-RFC's preference for a preexisting gap of over 5-nt ssDNA and suggest a direct role of the 9-1-1 in gap repair with various TLS (*trans*lesion synthesis) polymerases in addition to signaling the ATR kinase.

Graphical Abstract

*Correspondence: odonnel@rockefeller.edu (M.E.O.), huilin.li@vai.org (H.L.).

AUTHOR CONTRIBUTIONS

M.E.O. and H.L. designed research; F.Z., R.E.G., and N.Y.Y. performed research; F.Z., R.E.G., N.Y.Y., M.E.O., and H.L. analyzed the data; and F.Z., M.E.O., and H.L. wrote the manuscript with input from all authors.

SUPPLEMENTAL INFORMATION

Supplemental information can be found online at https://doi.org/10.1016/j.celrep.2023.112694.

DECLARATION OF INTERESTS

The authors declare no competing interests.

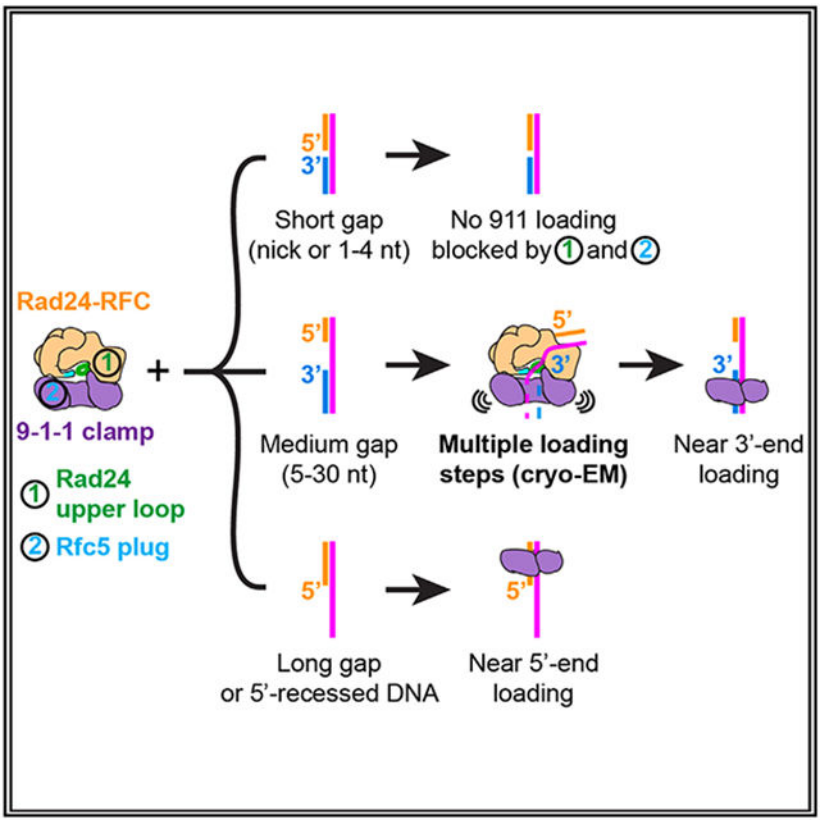

In brief

The prevailing view is that the 9-1-1 clamp is loaded by Rad24-RFC onto the DNA 5′ end to trigger the DNA damage checkpoint pathway. Zheng et al. report that 9-1-1 can also be loaded onto the 3′ end of a medium-size DNA gap.

INTRODUCTION

A human cell accrues up to 100,000 DNA lesions a day.[1] Left unrepaired, these lesions cause mutations and programmed cell death at the cell level and aging and cancers at the organismal level.[2-4] Fortunately, cells have evolved multiple DNA damage response mechanisms to detect and repair DNA damage and maintain genome integrity. One such mechanism is the cell-cycle checkpoint that encompasses an upstream damage signaling 9-1-1 DNA clamp, the associated clamp loader Rad24-RFC (replication factor C), and the downstream ATR-Chk kinases.[5-10] 9-1-1 transduces damage signals to these kinases to arrest cell-cycle progression from G1 to S during DNA replication in the S phase, or from G2 to M, in order to allow time for damage repair.[11-14] The 9-1-1 clamp is a heterotrimer composed of Rad9-Hus1-Rad1 in human and Ddc1-Mec3-Rad17 in *Saccharomyces cerevisiae* (*S.c.*).[15] 9-1-1 has a ring-like structure with a pseudo-6-fold symmetry that resembles a replicative DNA clamp.[16-19] However, all replicative DNA clamps are homo-oligomers, such as the homo-trimeric archaeal and eukaryotic PCNA (proliferating cell nuclear antigen),[20-22] the homo-dimeric *E. coli* β clamp,[23] and the homo-

trimeric T4 phage gp45 clamp.[24] The DNA replication sliding clamps stimulate activity and confer high processivity to their associated DNA polymerases and are also utilized by many other DNA metabolic enzymes.[16,25-27]

The canonical eukaryotic clamp loader is the RFC heteropentamer that loads PCNA clamps onto DNA.[28-30] However, eukaryotes also contain three alternative clamp loaders that contain four subunits in common with RFC but replace the Rfc1 subunit with another subunit, Egl1, Ctf18, or RAD17 (Rad24 in *S.c.*).[31] Rad24(RAD17)-RFC is distinct from the other clamp loaders, as it functions with the 9-1-1 clamp instead of PCNA. The PCNA and 9-1-1 DNA clamps are topologically closed and need to be opened by ATP-driven clamp loaders to encircle the DNA duplex.[25,32,33] The clamp loaders all have a similar two-tiered shallow spiral architecture, with five collar domains forming the top tier and five AAA+ modules forming the second tier that binds the C-terminal face of DNA clamps in the presence of ATP.[24,34-37] It has been established that RFC loads PCNA onto the DNA 3′ end by binding the DNA inside the ATPase chamber formed by the 5 subunits,[24,28-30,38] while Rad24-RFC loads 9-1-1 onto the 5′ end[39-41] by binding the 5′ DNA at an external site on the "shoulder" of Rad24.[42,43] Therefore, the two clamp loaders appear to use different DNA-binding sites to load their respective clamps onto the opposite ends of DNA.

In light of Rad24-RFC binding a recessed 5′ end, three recent studies have revealed that RFC too has an external 5′ end DNA-binding site on the external "shoulder" of Rfc1, comparable to the external site on Rad24 of Rad24-RFC, and that the external site is used for loading PCNA onto a nicked or a gapped DNA substrate for DNA repair.[28-30] This has prompted us to question whether Rad24-RFC loads 9-1-1 onto a gapped DNA, as previously published Rad24(RAD17)-RFC studies focused on 9-1-1 loading onto an isolated recessed 5′ end and not a gap containing both 3′ and 5′ ends.[40-44] The structure indicated that if 9-1-1 was loaded at gaps of around 10 nt, it would place 9-1-1 onto a 3′ primer junction for possible use by TLS (*trans*-lesion synthesis) polymerases, occurrences that biochemical studies have indicated.[45,46]

We find here that 9-1-1 is loaded onto gaps more efficiently than at an isolated recessed 5′ end, indicating that gaps formed during replication of damaged DNA could be used for 9-1-1 loading. However, Rad24-RFC is known to be unable to load 9-1-1 at a DNA nick, unlike RFC, which can load PCNA at nicks and any gap size.[28,29,41,47] To understand the gap size limitation of Rad24-RFC, we designed DNAs having either a 5- or 10-nt gap and assembled *in vitro* the Rad24-RFC–9-1-1-DNA ternary complex onto each gapped DNA in the presence of ATPγS. Our cryoelectron microscopy (cryo-EM) study of the *in-vitro*-assembled complexes captured multiple 9-1-1 loading intermediates at an average resolution better than 3 Å and revealed key structural features in Rad24-RFC that underlie the preexisting gap requirement for efficient 9-1-1 clamp loading. Overall, the study supports the idea that 9-1-1 is preferentially loaded at larger gaps and could therefore be predisposed to loading the 9-1-1 clamp onto 3′ DNA for both direct DNA repair and for ATR activation.

RESULTS

9-1-1 loading is more efficient at a gap than at a single 5′ end

Recent structural studies of RFC reveal details of how it can load PCNA onto nicked DNA and various gaps.[28-30] However, 9-1-1 clamp loading has focused on 5′ recessed ends having a 3′ single-stranded DNA (ssDNA) overhang with no gap and has not studied the efficiency of 9-1-1 loading at a gap vs. an isolated 5′ end.[39,41-43] Thus, we examined whether Rad24-RFC can load 9-1-1 onto gapped DNA and compared the efficiency with 9-1-1 clamp loading at an isolated 5′ end. For this assay, we utilized two primer oligos that hybridize to a longer template oligo to form a DNA having either a 10-nt gap or an isolated 5′ end (Figure 1A; Table S1). The template strand contained biotin at one end and DIG (digoxigenin) at the other, such that the DNA could be bound to streptavidin magnetic beads at one end and the Fab of a DIG antibody at the other end, to block 9-1-1 sliding off DNA. To follow 9-1-1 clamp loading, we tagged 9-1-1 with a 7-residue PKA kinase motif and used PKA kinase to label it using α^{32}P-ATP. The ^{32}P-9-1-1 clamp loading reaction was performed using Rad24-RFC and magnetic DNA-bead conjugates, and then the magnetic beads were washed to remove ^{32}P-9-1-1 not bound to DNA before quantitation by liquid scintillation. The results show that ^{32}P-9-1-1 is loaded onto a 10-nt gap more efficiently than at an isolated 5′ end (Figure 1B). Reactions lacking DNA, Mg^{2+}, or Rad24-RFC gave no significant ^{32}P-9-1-1 loading, consistent with active ATP-dependent 9-1-1 clamp loading onto the DNA by Rad24-RFC (Figure 1B).

While RFC can load PCNA at nicks and any gap size, Rad24-RFC has been shown to be incapable of loading 9-1-1 at a nick.[28,29,41,47] Hence, we examined the ability of Rad24-RFC to load 9-1-1 onto gaps of different sizes. The results show that while Rad24-RFC does not load 9-1-1 at a nick or a 1-nt gap, it is capable of loading 9-1-1 onto gaps of 5–30 nt (Figure 1C). The presence of RPA (replication protein A) did not change the results significantly but appeared to stimulate the reaction some-what as the gap size increased. Considering that a 1-nt gap is not utilized by Rad24-RFC/9-1-1, one may conclude that short base excision gap repair does not utilize 9-1-1. However, 9-1-1 loading at gaps of 5 nt or more indicates that 9-1-1 may be utilized in long base excision gap repair, or nucleotide excision repair (see discussion).

When the 9-1-1 clamp is loaded onto 5′ ends, it signals the cell-cycle checkpoint, but numerous 5′ ends are formed during normal lagging strand replication in the absence of damage, occurring every 100–200 bp.[48] Thus, one may question how the cell prevents Rad24-RFC from utilizing these numerous 5′ sites that could potentially result in cell-cycle arrest? To address this, we compared the kinetics of RFC loading of PCNA onto DNA and Rad24-RFC loading of 9-1-1 onto DNA. The results show that RFC/PCNA loading is an order of magnitude more rapid than Rad24-RFC–9-1-1 (Figure 1D). Therefore, we propose that during normal replication, Okazaki fragments are filled in and ligated faster than 9-1-1 loading could occur. This proposal is based on recent elegant studies[49] that indicate that Pol δ/PCNA/Fen1/ligase is exceedingly rapid in completing Okazaki fragment maturation. Therefore, Rad24-RFC may not have time to load 9-1-1 onto 5′ ends of lagging strand fragments during unobstructed DNA replication.

Cryo-EM structure of Rad24-RFC–9-1-1 assembled on a 10-nt gapped DNA substrate

To examine the structure of 9-1-1 loading onto a 10-nt gapped DNA, we mixed separately purified Rad24-RFC and the 9-1-1 clamp with a 10-nt gapped DNA substrate (Figure 2A) at a molar ratio of 1:1.2:1.6 and in the presence of 0.5 mM weakly hydrolysable ATP analog ATPγS and 5 mM Mg^{2+} (see STAR Methods for details). The mixture was used directly to make cryo-EM grids without further purification. 2D class averages of selected particle images showed successful reconstitution of the Rad24-RFC–9-1-1 clamp–10-nt gapped DNA complex (Figure S1A). After multiple rounds of 2D and 3D classifications, 3D reconstruction, and non-uniform refinement using cryoSPARC[50] and Relion,[51] we obtained five EM maps. These maps had a similar dimension of 129 × 113 × 108 Å and had an average resolution range of 2.76 to 2.94 Å (Figures S2 and S3).

We built atomic models for all five maps based on published structures of Rad24-RFC–9-1-1 bound to a 5′ tailed DNA[42,43] and refined these models to < 3-Å resolution (Table 1). The overall architecture of the five Rad24-RFC–9-1-1-10-nt gapped DNA complex structures are similar to previously reported clamp–clamp loader complexes.[24,35,36,38,42,43] They all adopt the expected three-tiered architecture, with Rad24-RFC forming the top (collar domains) and middle (AAA+ modules) tiers that sit above 9-1-1 at the bottom tier (Figures 2A and 2B). The 10-nt gapped DNA used in this study contains three regions: the 3′ ss/double-stranded (ds) junction (primer1/template DNA), the middle 10-nt ssDNA gap (residues 21–30 nt of the template strand), and the 5′ ss/ds junction (primer2/template DNA) (Figure 2A). In all five structures, the 5′ ss/ds junction DNA is stably bound to the external shoulder of Rad24, and the Rad24-RFC loader is highly similar, with a root-mean-square deviations (RMSDs) between main-chain C_α atoms ranging from 0.6 to 0.7 Å (Video S1).

Logically, these structures represent the Rad24-RFC–9-1-1 clamp–10-nt gapped DNA complex in five different DNA binding and clamp loading stages: we assigned the 2.93-Å-resolution structure with an open 9-1-1 clamp but without the 3′ ss/ds junction DNA as the step 1 intermediate; the 2.94-Å-resolution structure with an open 9-1-1 and partially bound 3′ ss/ds junction DNA as the step 2 intermediate; the 2.76-Å-resolution structure with an open 9-1-1 and with stably bound 3′ ss/ds junction DNA density as the step 3 intermediate; the 2.90-Å-resolution structure with a gate partially closed 9-1-1 as the step 4 intermediate; and the 2.85-Å-resolution structure with a gate fully closed 9-1-1 encircling the 3′ ss/ds junction DNA as the step 5 intermediate (Figure 2B).

The Rad24 upper loop blocks the 3′ ss/ds junction and sets the minimum ssDNA gap size

Rad24-RFC recognizes the DNA within its internal chamber (i.e., 3′ ss/ds junction DNA) in a similar manner as the yeast RFC.[29,30,38] The α-helices 4 and 5 (α4 and α5) in the AAA+ modules of all Rad24-RFC subunits wrap around and trace the template strand of 3′ ss/ds junction DNA, forming H-bonds with the template phosphate backbone (Figure 3B). For example, Rad24 Met-163, Rfc5 Arg-106, Rfc4 Arg-90, Rfc3 Ile-90 and Arg-94, and Rfc2 Ile-103 and Arg-107 of α4 helices form H-bonds with the template strand, and Rfc3 Thr-123 of the α5 helix forms an H-bond with the template strand. The loader has only very limited interactions with the 3′ primer strand (i.e., Rad24 Arg-199 of α5 and Asn-80 of the Rfc5 plug form H-bonds with that strand) (see also Figure S4C).

In the previously reported DNA-bound structures,[42,43] there were two structural elements in Rad24-RFC that appeared to be narrowing the DNA path: a β-hairpin coming from Rcf5 (also termed RFC5 E-plug) and a long loop positioned at the upper part of the inner chamber coming from Rad24 (termed upper loop). We therefore hypothesized that these structural elements might be responsible for the DNA-binding behavior of Rad24-RFC. In this study with the 10-nt gapped DNA, we found that a dsDNA segment—the 3′ ss-/dsDNA—can actually be accommodated into the lower chamber of Rad24-RFC, with the 3′ junction residing just below the upper loop (Figure 3A).

Interestingly, we found that it is the Rad24 upper loop that is primarily responsible for blocking the 3′ junction, thereby preventing the duplex region of the DNA from advancing further up the central channel (Figures 3B and S4A; Video S2). The Rfc5 E-plug can accommodate dsDNA and apparently plays an accessory role to the Rad24 long loop. Of the 10-nt poly(dT) ssDNA gap used in our DNA substrate, up to seven nucleotides could be modeled based on electron density: in both step 3 and 5 structures, we modeled four nucleotides adjacent to the 3′ ss-/dsDNA junction and three nucleotides near the 5′ ss-/dsDNA junction; the 22-Å density gap can be connected by three additional nucleotides, accounting for the total 10-nt poly(dT) ssDNA in the template strand DNA (Figure 4A, bottom middle). A 9-nt ssDNA distance between a sensor chip and a 5′ end was previously shown to enable 9-1-1 loading by Rad24-RFC, consistent with the current study.[41]

Explanation for inability of Rad24-RFC to unwind DNA like the canonical RFC

RFC was recently shown to harbor a separation pin (Rfc1 Trp-638) to unwind dsDNA from a 3′ ss-/dsDNA junction[29,38] and is capable of unwinding a nicked dsDNA to form a 6-nt ssDNA gap for PCNA loading using ATPγS, achieved by clamp loader-to-DNA binding energy and not requiring hydrolysis.[28] A side-by-side comparison of the Rad24-RFC–9-1-1–DNA structure (step 5) with several structures of the replicative clamp loader–clamp–DNA complexes reveals two striking distinctions (Figures 3B-3F, S4B, and S5). First, the upper loop of Rad24 is much longer than corresponding loops of the *S.c.* RFC and the *E. coli* clamp loader, and the T4 clamp loader lacks an equivalent loop. Second, while all replicative clamp loaders possess a DNA duplex separation pin (i.e., Trp-638 in yeast Rfc1, Tyr-316 in *E. coli* $\delta\gamma_3\delta'$, and Phe-63 in T4 phage gp44/62 clamp loader),[24,29,52] a similar duplex separation pin is absent in Rad24. Further, the Rad24 loop that lacks the separation pin is located much higher within the central chamber than the corresponding loops in the replicative clamp loaders harboring the separation pin. By superimposition, we found that the 3′ junction of the primer/template in all replicative loader complexes (RFC, *E. coli* $\delta\gamma_3\delta'$, and T4 loader) would clash with the Rad24 long upper loop (Figures 3C-3E, S4B, and S5). Based on these observations, we suggest that Rad24-RFC has evolved the long upper loop to specifically stop the 3′ ss/ds primer template junction at just below this loop, thereby enforcing a minimum ssDNA gap size (i.e., ssDNA region in the template strand between the lower 3′ junction and the upper 5′ junction of the gapped DNA). We further suggest that because the 3′ junction is blocked in Rad24-RFC and no longer requires unwinding, Rad24 has lost the separation pin during evolution. Consistent with the presence of 3′ junction unwinding activity of the replicative clamp loaders and the absence of an unwinding activity of Rad24-RFC,[29,38-41] there is a side tunnel in yeast RFC from which the

unwound primer 3′ tail emerges, but this tunnel is narrower and is blocked at the bottom by the Rad24 upper loop in Rad24-RFC (Figure S6A and S6B).

Five intermediate structures reveal a top-to-bottom binding process in loading 9-1-1 onto a 10-nt gapped DNA

As mentioned above, in those five 10-nt gapped DNA-bound intermediates, the upper loop of Rad24-RFC interacts with 5′ ss/ds junction DNA similarly; the main differences lie in the size of the DNA entry gate of 9-1-1 and the binding of the 3′ ss/ds junction DNA in the central chamber of the loader (Figure 4A). In the step 1 structure, the 9-1-1 DNA gate is 42 Å wide, and only four nucleotides in the 10-nt ssDNA gap region near the 3′ junction are visible. In the step 2 structure, the 9-1-1 gate remains wide open. There is relatively weak DNA density in the loader chamber as well as inside the 9-1-1 clamp, and the density is broken at the interface between the loader and the clamp. In the step 3 structure, the chamber DNA is stably bound with strong density (P1 6–20 and T 31–45 with a 15-bp dsDNA region), although the 9-1-1 gate is still open. In the step 4 structure, the 9-1-1 gate starts to close around the stably bound 3′ ss/ds junction DNA in the chamber of the loader, as the gate has narrowed to 19 Å. In contrast, the 9-1-1 gate is totally closed around the DNA in the step 5 structure (Figure 4A).

It is clear from the above description that DNA binding is a three-stage top-to-bottom process that starts with the 5′ ss/ds junction binding to the external shoulder site of Rad24-RFC on the top. This is followed by the gap ssDNA region and the top region of the 3′ ss-/dsDNA junction DNA entering the inner chamber of Rad24-RFC through the A-gate (Figure 2B, top left) that is open between the Rad24 N-terminal AAA+ module and the C-terminal A′ domain (step 1). And finally, the 3′ ss-/dsDNA region enters the 9-1-1 central channel (steps 2–3).

9-1-1 gate closure accompanies the binding of the 3′ chamber DNA

We next performed a flexibility analysis of the five loading intermediates to understand the relationship between DNA binding and 9-1-1 gate closure. We used the B factors of the atomic models, a measurement of thermal motion, as an indicator of the structural flexibility (Figure 4A). In the step 1 structure, the 5′ ss/ds junction DNA at the external shoulder site of Rad24 is stably bound except at the terminus (orange), and the gate-lining subunits Ddc1 and Mec3 of 9-1-1 are partially flexible (light yellow), but the third 9-1-1 subunit (Rad17) is stable (light blue). The 42-Å-wide gap in 9-1-1 is more than sufficient to allow passage of the 20-Å-wide duplex of the 3′ ss/ds junction DNA into the central chamber of the loader. In the step 2 structure, both 3′ ss/ds junction DNA in the chamber (orange to red) and 9-1-1 (yellow) become more flexible as the 3′ ss/ds junction DNA is entering the clamp. This is compared with the step 3 structure, in which both DNA and the 9-1-1 gate become stabilized upon completion of DNA entrance in step 2. Interestingly, in the step 4 structure, the DNA gate is only 19 Å wide, and not only the gate-lining Ddc1 and Mec3 (yellow) but also the 3′ ss/ds junction DNA (red) in the chamber become flexible. This is probably due to the perturbation by Mec3 movement to close the 9-1-1 gate. As expected, both 9-1-1 (light blue) and DNA (light yellow to light blue) are stabilized in the DNA fully bound and gate fully closed step 5 structure. Therefore, we conclude that 9-1-1 gate closure progresses along

with the gradual insertion and eventual stable binding of the 3′ ss/ds junction DNA in the chamber. Taken together, we suggest that the five intermediates captured by cryo-EM can be considered a temporal and sequential loading process of the 9-1-1 clamp onto a gapped DNA by Rad24-RFC.

Mec3 functions as the DNA entry gate of the 9-1-1 clamp

We noticed that both gate-lining subunits Mec3 and Ddc1 are flexible during the gate closure process, but the flexibility of Mec3 is significantly more pronounced than Ddc1 (Figure 4A), particularly in the step 4 structure where the gate has partially closed (compare the yellow-to-orange Mec3 with the light yellow Ddc1) and in the step 5 structure with a fully closed 9-1-1 gate (compare the white Mec3 with the blue Ddc1). This observation implies that gate closure may be asymmetric in that the two gate subunits contribute unequally to the clamp closing process. To investigate this more quantitatively, we superimposed the 9-1-1 clamps in steps 1–4 with the gate-closed 9-1-1 clamp in step 5 and calculated their respective $RMSD_{C\alpha}$ and colored the clamps by their respective $RMSD_{C\alpha}$ values (Figure 4B). The results show that 9-1-1 gate opening is mediated by an in-plane ~42° rigid-body rotation of Mec3 pivoting on the interface region between Mec3 and Rad17 (steps 1–3). Therefore, the partial gate closure in step 4 is accomplished by Mec3 rotating back toward Ddc1 by 30°. The final gate closure from step 4 to step 5 involves another 12° rotation of Mec3 to contact Ddc1 (Figure 4B). Therefore, we suggest that Ddc1 is largely stationary and that the 9-1-1 gate opening and closure is primarily mediated by a rigid-body rotation of Mec3.

The 9-1-1 clamp ring remains flat during gate opening and closure

The 9-1-1 DNA clamp studies thus far have only observed flat ring structures when alone or encircling dsDNA.[31] However, during loading of DNA replication clamps onto DNA, the clamp is cracked open by the clamp loaders and forms a lock washer-like spiral structure, exemplified by the PCNA lock washer being loaded onto DNA by RFC,[28,29,47] as well as the T4 clamp lock washer being loaded onto DNA by the T4 clamp loader[24,33] (Figure S7). However, in all five steps of 9-1-1 clamp loading onto DNA by Rad24-RFC, the 9-1-1 clamp remains flat, despite its various degrees of gate opening (Figures 2, 4, and S7; Video S3). Therefore, the in-plane mechanism of gate opening/closure of the 9-1-1 clamp appears to be distinct. In fact, 9-1-1 is the only clamp ring composed of three different subunits; the bacterial and eukaryotic cellular replicative DNA clamps are either homo-dimeric or homo-trimeric and open out of plane. Further study is needed to understand if the heteromeric structural feature is responsible for the in-plane gate opening/closure mechanism of the 9-1-1 clamp.

Rad24-RFC binds DNA differently at a 5-nt gap

As explained above, the structure of Rad24-RFC suggests that the upper loop will limit the size of gap that 9-1-1 can be loaded on. Therefore, we next imaged the mixture of Rad24-RFC, 9-1-1, and a 5-nt gapped DNA (Figure 5A) in the presence of ATPγS, prepared in the same condition as with the 10-nt gapped DNA. 2D and 3D classification of cryo-EM images showed that most Rad24-RFC–9-1-1 complex particles did not contain DNA (Figure S1B). For the particles with some DNA density in the central chamber of Rad24-RFC, focused

refinement around DNA showed that the DNA density was either partial or distorted from the B-form structure in 4 out of the 5 subclasses. Further refinement of the subclass with undistorted and relatively strong DNA density resulted in the final 3D map at 3.04-Å overall resolution (Figure S3F, S3G, and S8). We observed a lower percentage of DNA-loaded particles using 5-nt gapped DNA vs. 10-nt gapped DNA, consistent with the somewhat lower, but repeatable, extent of loading 9-1-1 onto 5-nt gap DNA compared with loading of 9-1-1 at larger gaps in Figure 1. This observation indicates that Rad24-RFC has difficulty loading 9-1-1 onto a 5-nt gapped DNA vs. 10-nt gapped DNA.

The 5-nt gapped DNA-bound Rad24-RFC–9-1-1 structure resembles the step 5 structure of the 10-nt gapped DNA-bound complex. The overall structures are nearly superimposable with an RMSD of main-chain C_α atoms of 0.6 Å, and both 9-1-1 clamps are fully closed (Figures 5B and S9; Video S1). The three intermediate steps 2–4 seen using the 10-nt gapped DNA were not observed using the 5-nt gapped DNA. Hence, it is possible that the intermediate states of the 9-1-1 ring using the 10-nt gapped DNA are nearly isoenergetic forms and stochastic in nature and that these states are not stable at a strained 5-nt gapped DNA, resulting in only the closed form.

An important difference is observed in the 3′ ss-/dsDNA within the central chamber (Figure 5C). This DNA region was rotated 180° around the helical axis compared with the 10-nt gapped DNA (Figure 5D). In the rotated pose, the template strand is oriented the closest to the upper 5′ shoulder DNA, enabling the short 5-nt ssDNA to bridge the gap between the two dsDNA segments. Interestingly, the Rfc5 hairpin plug now contacts the minor groove of the rotated 3′ ss-/dsDNA of the 5-nt gapped DNA, distorting the DNA and, in contrast with the Rfc5 plug, contacting the major groove of the chamber DNA of the 10-nt gapped DNA. However, the Rad24 upper loop is in a similar position in the two structures, blocking the upward advance of the 3′ ss-/dsDNA segment. Therefore, no unwinding of either the 3′ or 5′ dsDNA ends of the 5-nt gapped DNA was observed, underscoring the absence of separation pins in the Rad24-RFC clamp loader as described above. In summary, the 5-nt gapped DNA-bound structure reveals a possible cooperation between the Rfc5 plug and the Rad24 upper loop in controlling the minimal DNA gap size accessible to Rad24-RFC and confirms the absence of DNA unwinding activity in Rad24-RFC.

DISCUSSION

9-1-1 loading is more efficient on a gapped DNA vs. 5′ recessed DNA

The current study shows that Rad24-RFC is more efficient in loading the 9-1-1 clamp onto a gapped DNA compared with an isolated recessed 5′ DNA terminus. Indeed, our cryo-EM structural results show that the 3′ duplex of gapped DNA binds in the central channel of Rad24-RFC, compared with exclusively ssDNA in the case of an isolated recessed 5′ DNA. It therefore seems likely that the enhanced 9-1-1 loading at gaps vs. single 5′ ends may be due to Rad24-RFC binding the 5′ dsDNA at the same time as the 3′ ss-/dsDNA at gaps. This geometry predicts that the 9-1-1 clamp will be loaded around a 3′ primer terminus instead of ssDNA. In this case, the 9-1-1 clamp is positioned at a 3′ ss-/dsDNA (similar to PCNA) and could be used by TLS Pols as indicated in earlier studies[53-55] and as described further below. We presume that most DNA lesions on the lagging strand template during

replication will result in stopping Pol δ–PCNA and thus require TLS Pols or recombinative repair to bypass the lesion, extending the time of Okazaki fragment gap fill in. Thus, lagging strand gaps might be a major source of 5′ ends for 9-1-1 loading and cell-cycle arrest during DNA damage in S phase.

A proposed model for 9-1-1 loading onto a gapped DNA

Based on previous biochemical and structural studies of this system,[39-43] recent structural knowledge of PCNA loading by RFC,[28-30,38] and our current 9-1-1 clamp loading intermediates (steps 2–4) described above, we propose here a significantly more detailed 9-1-1 loading process, specifically onto gapped DNAs by Rad24-RFC (Figure 6A). Before encountering a DNA, we suggest that the 9-1-1 ring is opened by Rad24-RFC in the presence of ATP, in a mechanism resembling the PCNA gate opening by RFC in the absence of DNA (Figure S7).[38] Consistent with this suggestion, it has been shown that in the presence of ATP or ATPγS, Rad24-RFC and the 9-1-1 clamp can form a complex without a DNA substrate,[39,40] although an experimental structure of Rad24-RFC with an open 9-1-1 ring in the absence of DNA has yet to be captured. In step 1, we suggest that Rad24-RFC first engages the 5′ duplex at the external (shoulder) DNA-binding site of Rad24. This is followed by steps 2 and 3, in which the ssDNA at the gap as well as the 3′ ss-/dsDNA region gains access to the Rad24-RFC central chamber and the 9-1-1 central channel to become stably bound there. We further suggest that during this top-to-bottom DNA-binding process, the Rad24 upper loop plays a crucial role in selecting against binding a DNA substrate with a ssDNA gap less than 5 nt. In step 4, Mec3 rotates toward Ddc1 to close the DNA entry gate in 9-1-1. In step 5, we suggest that the 9-1-1 gate closing on the stably bound DNA will activate the ATPase activity in Rad24-RFC, leading to ATP hydrolysis, release of inorganic phosphate, and the dissociation of ADP-bound Rad24-RFC. These actions leave the closed 9-1-1 clamp encircling 3′ duplex DNA (step 6).

Loading of 9-1-1 on 5′ sites by Rad24-RFC is much slower than PCNA loading by RFC

We demonstrate here that 9-1-1 clamp loading at a 10-nt DNA gap is much slower than RFC loading PCNA at the same gap (Figure 1B). This finding is consistent with the different ATPase activity of human Rad17-RFC compared with human canonical RFC at a 5′ ss-/dsDNA.[39] Thus, when normal repair pathways of a cell are not “overloaded,” PCNA is likely assembled onto gapped DNA and utilized for repair rather than a 9-1-1 clamp that may be utilized to activate the DNA damage checkpoint and shut down the cell cycle. Presumably, in the event of significant DNA damage, the 9-1-1 clamp is loaded at stalled and incomplete Okazaki fragments or DNA repair gaps to signal the DNA damage response and to halt the cell cycle to gain time to repair DNA before continuing the cell cycle.

Possible physiological consequences of the different DNA structures used by Rad24-RFC and RFC

The replicative clamp loader RFC is well known to load PCNA at a 3′ recessed DNA end, the normal primer for DNA synthetic extension.[32] In contrast, Rad24-RFC has been established to load the damage signaling 9-1-1 clamp onto a 5′ recessed DNA.[39,41] However, three recent structural studies on RFC have broken the established norm, revealing the 5′ recessed DNA-binding capacity on the shoulder of the Rfc1 subunit of RFC and the

loading of PCNA onto a gapped DNA (at the 3′ end) where both 3′ and 5′ recessed ends are present.[28-30] The current study shows the Rad24-RFC, like RFC, is also able to load 9-1-1 onto a gapped DNA by simultaneously binding to both the 5′ and 3′ recessed DNA. This raises the question of whether there is any significant mechanistic difference in loading their respective clamps onto gapped DNA substrates. Based on the current structural and biochemical information, we suggest two major differences (Figure 6B). Firstly, Rad24-RFC cannot unwind dsDNA and thus requires a preexisting ssDNA gap of a minimum length of 5 nt for efficient loading, whereas RFC can unwind DNA and even load PCNA at nicks, due to its ability to unwind DNA at a nick or small DNA gaps.[28-30] Secondly, Rad24-RFC may be evolved to prefer ssDNA gaps so as not to trigger a cell-cycle checkpoint over nicks that can be sealed by ligase or dealt with by short gap base excision repair (i.e., a 1-nt gap).

In overview, eukaryotes have evolved different clamp loaders to efficiently maintain genome integrity. For many short ssDNA patches (<5-nt gap) produced during base excision pathways, RFC is likely utilized to load PCNA to these sites and then goes on to recruit a translesion synthesis polymerase (e.g., Pol β, Pol ε, Pol ζ, and Rev1) to fill in the short gaps, followed by the action of a ligase to seal the nick and complete repair.[53-55] Rad24-RFC seems to be reserved for ssDNA patches of ≥5 nt. This might enable eukaryotic cells to efficiently repair very short gap DNA damage without triggering the cell-cycle 9-1-1-activated ATR kinase route that might be more important when extensive damage and longer ssDNA gaps occur. However, it is interesting to note that 9-1-1 interacts with Pol ζ to reduce Pol ζ-dependent spontaneous mutagenesis[45] and with Pol ε to increase the catalytic efficiency for correct nucleotide incorporation.[56] Furthermore, 9-1-1 interacts with TopBP1 and DNA polymerase-α directly at stalled DNA replication forks[57] and with Pol β to stimulate its activity.[46] Therefore, 9-1-1 likely has a broader role that functions beyond DNA damage signaling. The ability of Rad24-RFC to load 9-1-1 clamps at 5- to 10-nt gaps indicates that the 9-1-1 clamp will be left (after clamp loader ejection) to encircle the 3′ duplex, not the 5′ duplex, of the medium-sized gaps, and this places its orientation on DNA to favor action with DNA polymerases to fill in gaps produced by DNA damage.

Limitations of the study

The current study has revealed a multi-step loading mode of the 9-1-1 clamp onto—unexpectedly—the 3′ end DNA of a medium-sized gap (5–30 nt) by the alternative clamp loader Rad24-RFC. However, we have not determined the size of the smallest gap(s) onto which the 9-1-1 clamp can be loaded. We are also unsure how the dsDNA inside the Rad24-RFC chamber will be oriented when the gap size is larger than 5 nt but smaller than 10 nt, i.e., whether the axial or azimuthal orientation of the DNA will take on one of the two orientations as observed for the 5- and 10-nt gapped substrates or other orientations. Despite these limitations, the study has enabled us to propose a function for 9-1-1 in DNA damage repair, specifically that this process may enable the use of the 9-1-1 clamp by DNA polymerases for gap repair. The proposed function needs further *in vivo* studies. However, a more detailed understanding also requires more extensive biochemical, biophysical, and structural investigation.

STAR★METHODS

RESOURCE AVAILABILITY

Lead contact—Further information and requests for reagents and resources may be directed to, and will be fulfilled by the Lead Contact Huilin Li (Huilin.Li@vai.org).

Materials availability—All plasmids used in this study will be available from the lead contact upon request. All cell lines used to express the proteins used in this study are available upon request without restrictions, although an MTA may be required.

Data and code availability

- The five EM maps of the *S. cerevisiae* Rad24-RFC–9-1-1 clamp–10-nt gapped DNA complex (steps 1–5) and one EM map of the Rad24-RFC–9-1-1 clamp–5-nt gapped DNA complex have been deposited in the Electron Microscopy DataBank with accession codes EMD-29412, EMD-29413, EMD-29414, EMD-29415, EMD-29416 and EMD-29417 respectively. Their corresponding atomic models have been deposited in the Protein DataBank with accession codes 8FS3, 8FS4, 8FS5, 8FS6, 8FS7, and 8FS8. These data will be publicly available as of the date of publication.
- This paper does not report original code.
- Any additional information required to reanalyze the data reported in this work will be available from the lead contact upon request.

EXPERIMENTAL MODEL AND STUDY PARTICIPANT DETAILS

Bacterial strains—The expression plasmids of *S.c.* Rad24-RFC, 9-1-1 clamp and RPA were generated by standard molecular biology techniques, constructed using the DH5α strain of *E. coli* (Thermo Fisher Scientific), and are listed in the key resources table. Those three multiprotein complexes were purified from the BL21(DE3) strain of *E. coli* (Thermo Fisher Scientific). *E. coli* strains were cultured in LB media.

METHOD DETAILS

Protein expression and purification—Rad24-RFC and the 9-1-1 clamp were expressed and purified as described in our earlier report.[43] RPA was purified as described in.[69]

Magnetic bead-based 9-1-1 clamp loading assays—S.c. 9-1-1 having an N-terminal 7-residue kinase recognition sequence on Mec3 was radiolabeled to a specific activity of approximately 70 cpm/fmol with [α-^{32}P] ATP (PerkinElmer Life Sciences, Inc) using the recombinant catalytic subunit of cAMP-dependent protein kinase produced in *E. coli* (a gift from Dr. Susan Taylor, University of California at San Diego) as described.[58] Protein concentrations were determined by Bradford assay reagent (Bio-Rad) using BSA as a standard. The oligonucleotides used to make the DNA substrates in this report (Table S1) were synthesized and PAGE purified or HPLC purified by Integrated DNA Technologies. To form the isolated nicked and gapped templates, 2500 pmol of each of primer #1 and

primer #2 were mixed with 1250 pmol of the template strand in 45 μL of Buffer A (5 mM Tris-HCl, 150 mM NaCl, 15 mM sodium citrate, final pH 8.5), then incubated in a 95°C water bath and cooled to room temperature (23°C) over a 30-min interval. 200 pmol of the annealed primed templates were combined with 1 mg of Dynabeads M-280 Streptavidin beads (ThermoFisher Scientific) in 200 μL of Buffer B (40 mM HEPES-NaOH pH 7.5, 0.1 mg/mL BSA, 1 mM DTT, 8 mM $MgCl_2$ and 120 mM NaCl) and incubated at 23°C for 30 min with agitation. Supernatant containing excess unbound primer oligonucleotides was removed using a magnetic separator. The DNA-beads were washed twice with 250 μL Buffer C (30 mM HEPES-NaOH pH 7.5, 1 mM DTT, 1 mM CHAPS) with 7 mM $MgCl_2$ and 100 mM NaCl, and then resuspended in 100 μL of the same buffer. The concentration of DNA conjugated to the beads was determined by measuring absorbance at 260 nm using a nanodrop spectrophotometer and was typically in the range of 1.0–2.0 pmol DNA per μl bead mix.

Before the start of the 9-1-1 loading assay, the Dig at the end of the DNA-bead conjugate was first blocked with anti-digoxigenin Fab fragment (Roche) in a ratio of 1:2 respectively in Buffer C with 7 mM $MgCl_2$. After the mixture was incubated at room temperature for 15 min with agitation, RPA was added to the DNA-bead conjugate in a ratio of 4:1 and incubated at 30°C for 5 min. The supernatant containing excess unbound Fab fragments and RPA was then removed using a magnetic separator. The blocked DNA-beads were resuspended in the following clamp loading mixture. Each reaction contained 100 nM antibody-blocked DNA-bead conjugate, 200 nM ^{32}P-9-1-1 in 50 μL of Buffer C with 8 mM $MgCl_2$, 50 mM NaCl and 1 mM ATP. The clamp loading reaction was initiated with 174 nM Rad24-RFC and incubated at 30°C with agitation for 5 min. The reaction was stopped by quenching with 25 mM EDTA on ice. The beads were then isolated with a magnetic separator and free protein was washed away with two washes of 250 μL Buffer C containing 100 mM NaCl. The DNA-bound radioactive 9-1-1 was stripped from the beads with 0.5% SDS and 5 min of boiling. One-half (25 μL) of the supernatant was then counted by liquid scintillation and quantitation was multiplied by two for quantitation of the full reaction.

For the time course comparison of PCNA loading versus 9-1-1 loading, the 10-nt gapped DNA was used and each reaction contained 100 nM antibody-blocked DNA-bead conjugate, 200 nM ^{32}P-PCNA or 200 nM ^{32}P-9-1-1 and 150 nM RFC or 150 nM Rad24-RFC in 50 μL of Buffer C with 8 mM $MgCl_2$ and 1 mM ATP. The PCNA loading reactions were incubated on ice for 0 to 25 s before being quenched with 25 mM EDTA. The 9-1-1 loading reactions were also incubated on ice but for longer times (0–4 min) before being quenched with EDTA. The amount of radiolabeled clamp loaded in each reaction was determined as described above.

Cryo-EM grids preparation and data collection—The 10-nt gapped DNA substrate with both 3′- and 5′- junctions, and its sequence is shown in Figure 2A. This DNA is the same as used in the biochemical assays as described above and was prepared as described previously.[29] The *in vitro* assembly of yeast Rad24-RFC–9-1-1 clamp–10-nt gapped DNA complex followed our previous procedure for reconstituting yeast Pol δ–PCNA–DNA complex.[70] Briefly, 6.6 μL purified 9-1-1 protein at 5.0 μM and 3.7 μL gapped DNA at 11.2 μM were mixed and incubated at 30°C for 10 min, then the mixtures, along with 0.75

μL 10 mM ATPγS and 0.75 μL 100 mM Mg-Acetate, were each added into 3.2 μL purified Rad24-RFC protein at 8.6 μM concentration, the final concentrations of the components were: Rad24-RFC at 1.8 μM, 9-1-1 clamp at 2.2 μM, 10-nt gapped DNA at 2.8 μM, ATPγS at 0.5 mM, and Mg-Acetate at 5 mM; the total reaction volume was 15 μL. The final molar ratio of Rad24-RFC: 9-1-1 clamp: DNA was 1.0: 1.2: 1.6. The mixture was then incubated in an ice-water bath for 1.5 h. Assembly of Rad24-RFC–9-1-1 clamp with the 5-nt gapped DNA (Figure 5A) followed the same procedure as the 10-nt gapped DNA, except that the gapped region is shortened to 5 (polydT$_5$).

The Quantifoil Cu R2/1 300 mesh grids were glow discharged for 1 min in a Gatan Solarus, then 3 μL of the mixture was applied onto the EM grids. Sample vitrification was carried out in a Vitrobot (Thermo Fisher Mark IV) with the following settings: blot time 2.5 s, blot force 3, wait time 3 s, inner chamber temperature 6°C with 95% relative humidity. The EM grids were flash-frozen in liquid ethane cooled by liquid nitrogen. Cryo-EM data were automatically collected on a 300 kV Titian Krios electron microscope controlled by SerialEM[59] in a multi-hole mode. The micrographs were captured at a scope magnification of 105,000×, with the objective lens under-focus values ranging from 1.3 to 1.9 μm, by a K3 direct electron detector (Gatan) operated in the super-resolution Video mode. During a 1.5 s exposure time, a total of 75 frames were recorded with a total dose of 64 $e^{-}/Å^2$. The calibrated physical pixel size was 0.828 Å for all digital micrographs.

Image processing and 3D reconstruction

The data collection and image quality were monitored by the cryoSPARC Live v3.1[50] installed in a local workstation. The image preprocessing including patch motion correction (on bin ×2 data), contrast transfer function (CTF) estimation and correction, blob particle picking (70–150 × diameter), and particle extraction (on bin ×4 data) were also achieved at the same time. A total of 19,603 raw micrographs for the 10-nt gapped DNA bound Rad24–RFC-911 complex was recorded during a three-day data collecting session (Figure S2). The extracted particle images were subjected to two rounds of 2-dimensional (2D) classification, resulting in a selected dataset of ~2.4 million “good” particle images. We also trained the automatic particle picking program Topaz[63] and used the trained model to pick up another particle dataset. The Topaz picked dataset was also subjected to two rounds of 2D classifications, resulting in a selected dataset of ~2.9 million “good” particle images. We then used the reported “Build and Retrieve” method to retrieve those less frequently occurring particle views.[71] The two particle datasets were combined by removing duplicates that were 40% overlapping (52 Å) or larger than the preset particle diameter (~130 Å). This resulted in a merged dataset of ~3.3 million particle images.

We performed ab initio 3D reconstruction with the combined dataset and obtained three initial maps in cryoSPARC. One map was chosen as reference for later 3D classification. The particle coordinates were transformed into Relion format[51] using the PyEM program.[72] At the same time, the collected raw images are imported into Relion 4.0, motion corrected by MotionCor2,[61] and CTF estimated and corrected by CTFFIND4.[62] Then, the particle images were re-extracted with the particle coordinates imported from cryoSPARC. We next performed 3D classification in Relion and obtained six 3D classes. One map lacked feature

and was considered “junk”, but the remaining 5 maps corresponded to different stages of 9-1-1 clamp loading by Rad24-RFC onto the 10-nt gapped DNA (Figure S2). After 3D auto-refinement, CTF refinement and Bayesian polish in Relion, the particles from each class were imported back to cryoSPARC for final non-uniform refinement, which resulted in five maps of the Rad24-RFC–9-1-1–10-nt gapped DNA complex. The map with an open 9-1-1 ring but lacking DNA density in the central chamber of Rad24-RFC was at 2.93 Å, the map with an open 9-1-1 ring and a weak chamber DNA density was at 2.94 Å, the map with an open 9-1-1 ring and a strong chamber DNA density at 2.76 Å, the map with a partially closed 9-1-1 ring and a strong chamber DNA density was at 2.90 Å, and the map with a fully closed 9-1-1 ring and a strong chamber DNA density was at 2.85 Å average resolution. All five maps had a 5′ DNA stably bound at the Rad24 external shoulder site (Figures S2 and S3).

A similar data collection and image processing strategy was used for the 5-nt gapped DNA bound Rad24-RFC–9-1-1 complex (Figure S8). We collected a dataset of 22,570 raw micrographs. The initial 3D reconstruction and heterogeneous refinement resulted in only two conformations, different from the five conformations of the 10-nt gapped DNA bound complex. One map was constructed from ~3.5 million particles and had an open 9-1-1 ring. This map had clear density for the 5′ shoulder DNA but had neither DNA density in the open 9-1-1 ring nor in the Rad24-RFC chamber. This map was essentially the same as the step-1 map we have solved for the 10-nt gapped DNA bound complex, thus was not processed further. The other map was reconstructed from about 2.1 million particles and had a closed 9-1-1 ring. This map had weak DNA density inside the Rad24-RFC chamber. To improve the chamber DNA density, we first performed 3D classification in cryoSPARC[50] and obtained 20 3D classes. Among the 20 maps, four had strong DNA density in the central chamber of Rad24-RFC and they were combined and imported into Relion[51] for further focused 3D classification around the chamber containing DNA region. We finally isolated a subpopulation of 242,906 particles with a relative stable chamber DNA density for final refinement, leading to the presented EM map at 3.04 Å average resolution (Figure S3F, S3G, and S8).

Model building, refinement, and validation—The previously reported cryo-EM structure of the yeast Rad24-RFC–9-1-1 clamp complexed with a shoulder DNA (PDB entry 7SGZ) was used as the starting model for atomic modeling of the six EM maps.[43] To model DNA in the central chamber of the clamp loader, we started with the 3′ ss/ds DNA-central chamber coordinates extracted from the structure of the yeast RFC–PCNA–2 DNA complex structure (PDB entry 7TFH), followed by manual adjustment. We also used the de novo modeling program Map-to-Model wrapped in PHENIX[68] and the module “Automated Nucleic Acid building” function integrated in COOT.[67] The two approaches led to similar gapped DNA models. The initial DNA model was first fitted into the most robust step-5 3D map of the 10-nt gapped DNA bound complex with the closed 9-1-1 ring, then merged as a single coordinate file in UCSF Chimera.[65] This served as the starting model for the step-5 EM map. The model was refined iteratively between the real space refinement in PHENIX and the manual adjustment in COOT. The atomic model of the step-5 complex was refined to 2.9 Å, and was comprehensively validated by the MolProbity program[73]

embedded in PHENIX. This model then served as the initial model for the four other 10-nt gapped DNA bound maps and the single 5-nt gapped DNA bound complex map. The model for each 3D map was subjected to a similar manual building process (Table 1). The step-1 and −2 maps with 10-nt gapped DNA had weaker EM densities for the two 9-1-1 gate subunits Ddc1 and Mec3, and the map of the 5-nt gapped DNA bound complex had weak 3′ ss/ds DNA density in the chamber. We used rigid body docking in these weak density regions, followed by manual adjustment in COOT and refinement by PHENIX. Structure figures were prepared using ChimeraX,[74] and assembled and labeled in Adobe Illustrator (Adobe Inc, San Jose, CA).

QUANTIFICATION AND STATISTICAL ANALYSIS

The quantification of clamp loading assay is based on the ^{32}P isotope labeled 9-1-1 or PCNA clamp, and each experiment using the magnetic bead assay of Figure 1 was carried out using three independently performed experiments. The data of Figure 1 are shown as standard error (SD) of the mean (SEM) performed by Microsoft Excel version 16.71. Gold Standard-Fourier Shell Correlation (GS-FSC) curves at the threshold of 0.143 were computed in cryoSPARC to determine the final resolutions of each cryo-EM density map. Statistical analysis of cryo-EM structure determination was generated during refinement with Phenix and can be found in Table 1. See more details in STAR Methods.

Supplementary Material

Refer to Web version on PubMed Central for supplementary material.

ACKNOWLEDGMENTS

Cryo-EM micrographs were collected at the David Van Andel Advanced Cryo-Electron Microscopy Suite at the Van Andel Institute. We thank G. Zhao and X. Meng for facilitating data collection. This work was supported by United States National Institutes of Health grants GM131754 (to H.L.) and GM115809 (to M.E.O.), the Van Andel Institute (US) (to H.L.), and the Howard Hughes Medical Institute (US) and BCRF 22-068 (US) (to M.E.O.).

REFERENCES

1. Giglia-Mari G, Zotter A, and Vermeulen W (2011). DNA damage response. Cold Spring Harbor Perspect. Biol 3, a000745. 10.1101/cshperspect.a000745.
2. Jackson SP, and Bartek J (2009). The DNA-damage response in human biology and disease. Nature 461, 1071–1078. 10.1038/nature08467. [PubMed: 19847258]
3. Yousefzadeh M, Henpita C, Vyas R, Soto-Palma C, Robbins P, and Niedernhofer L (2021). DNA damage—how and why we age? Elife 10, e62852. 10.7554/eLife.62852. [PubMed: 33512317]
4. Schumacher B, Pothof J, Vijg J, and Hoeijmakers JHJ (2021). The central role of DNA damage in the ageing process. Nature 592, 695–703. 10.1038/s41586-021-03307-7. [PubMed: 33911272]
5. Zhou BB, and Elledge SJ (2000). The DNA damage response: putting checkpoints in perspective. Nature 408, 433–439. 10.1038/35044005. [PubMed: 11100718]
6. Maréchal A, and Zou L (2013). DNA damage sensing by the ATM and ATR kinases. Cold Spring Harbor Perspect. Biol 5, a012716. 10.1101/cshperspect.a012716.
7. Blackford AN, and Jackson SP (2017). ATM, ATR, and DNA-PK: The Trinity at the Heart of the DNA Damage Response. Mol. Cell 66, 801–817. 10.1016/j.molcel.2017.05.015. [PubMed: 28622525]

8. Parrilla-Castellar ER, Arlander SJH, and Karnitz L (2004). Dial 9-1-1 for DNA damage: the Rad9-Hus1-Rad1 (9-1-1) clamp complex. DNA Repair 3, 1009–1014. 10.1016/j.dnarep.2004.03.032. [PubMed: 15279787]

9. Bermudez VP, Lindsey-Boltz LA, Cesare AJ, Maniwa Y, Griffith JD, Hurwitz J, and Sancar A (2003). Loading of the human 9-1-1 checkpoint complex onto DNA by the checkpoint clamp loader hRad17-replication factor C complex in vitro. Proc. Natl. Acad. Sci. USA 100, 1633–1638. 10.1073/pnas.0437927100. [PubMed: 12578958]

10. Gobbini E, Casari E, Colombo CV, Bonetti D, and Longhese MP (2020). The 9-1-1 Complex Controls Mre11 Nuclease and Checkpoint Activation during Short-Range Resection of DNA Double-Strand Breaks. Cell Rep. 33, 108287. 10.1016/j.celrep.2020.108287. [PubMed: 33086066]

11. Sancar A, Lindsey-Boltz LA, Unsal-Kaçmaz K, and Linn S (2004). Molecular mechanisms of mammalian DNA repair and the DNA damage checkpoints. Annu. Rev. Biochem 73, 39–85. 10.1146/annurev.biochem.73.011303.073723. [PubMed: 15189136]

12. Lanz MC, Dibitetto D, and Smolka MB (2019). DNA damage kinase signaling: checkpoint and repair at 30 years. EMBO J. 38, e101801. 10.15252/embj.2019101801. [PubMed: 31393028]

13. Niida H, and Nakanishi M (2006). DNA damage checkpoints in mammals. Mutagenesis 21, 3–9. 10.1093/mutage/gei063. [PubMed: 16314342]

14. Tannous EA, and Burgers PM (2021). Novel insights into the mechanism of cell cycle kinases Mec1 (ATR) and Tel1 (ATM). Crit. Rev. Biochem. Mol. Biol 56, 441–454. [PubMed: 34151669]

15. Venclovas C, and Thelen MP (2000). Structure-based predictions of Rad1, Rad9, Hus1 and Rad17 participation in sliding clamp and clamploading complexes. Nucleic Acids Res. 28, 2481–2493. 10.1093/nar/28.13.2481. [PubMed: 10871397]

16. Li H, Zheng F, and O'Donnell M (2021). Water skating: How polymerase sliding clamps move on DNA. FEBS J. 288, 7256–7262. 10.1111/febs.15740. [PubMed: 33523561]

17. Xu M, Bai L, Gong Y, Xie W, Hang H, and Jiang T (2009). Structure and functional implications of the human rad9-hus1-rad1 cell cycle checkpoint complex. J. Biol. Chem 284, 20457–20461. 10.1074/jbc.C109.022384. [PubMed: 19535328]

18. Doré AS, Kilkenny ML, Rzechorzek NJ, and Pearl LH (2009). Crystal structure of the rad9-rad1-hus1 DNA damage checkpoint complex–implications for clamp loading and regulation. Mol. Cell 34, 735–745. 10.1016/j.molcel.2009.04.027. [PubMed: 19446481]

19. Acharya S, Dahal A, and Bhattarai HK (2021). Evolution and origin of sliding clamp in bacteria, archaea and eukarya. PLoS One 16, e0241093. 10.1371/journal.pone.0241093. [PubMed: 34379636]

20. Madru C, Henneke G, Raia P, Hugonneau-Beaufet I, Pehau-Arnaudet G, England P, Lindahl E, Delarue M, Carroni M, and Sauguet L (2020). Structural basis for the increased processivity of D-family DNA polymerases in complex with PCNA. Nat. Commun 11, 1591. 10.1038/s41467-020-15392-9. [PubMed: 32221299]

21. Krishna TS, Kong XP, Gary S, Burgers PM, and Kuriyan J (1994). Crystal structure of the eukaryotic DNA polymerase processivity factor PCNA. Cell 79, 1233–1243. [PubMed: 8001157]

22. Gulbis JM, Kelman Z, Hurwitz J, O'Donnell M, and Kuriyan J (1996). Structure of the C-terminal region of p21(WAF1/CIP1) complexed with human PCNA. Cell 87, 297–306. 10.1016/s0092-8674(00)81347-1. [PubMed: 8861913]

23. Kong XP, Onrust R, O'Donnell M, and Kuriyan J (1992). Three-dimensional structure of the beta subunit of E. coli DNA polymerase III holoenzyme: a sliding DNA clamp. Cell 69, 425–437. 10.1016/0092-8674(92)90445-i. [PubMed: 1349852]

24. Kelch BA, Makino DL, O'Donnell M, and Kuriyan J (2011). How a DNA polymerase clamp loader opens a sliding clamp. Science 334, 1675–1680. 10.1126/science.1211884. [PubMed: 22194570]

25. Hedglin M, Kumar R, and Benkovic SJ (2013). Replication clamps and clamp loaders. Cold Spring Harbor Perspect. Biol 5, a010165. 10.1101/cshperspect.a010165.

26. Strzalka W, and Ziemienowicz A (2011). Proliferating cell nuclear antigen (PCNA): a key factor in DNA replication and cell cycle regulation. Ann. Bot 107, 1127–1140. 10.1093/aob/mcq243. [PubMed: 21169293]

27. Moldovan GL, Pfander B, and Jentsch S (2007). PCNA, the maestro of the replication fork. Cell 129, 665–679. 10.1016/j.cell.2007.05.003. [PubMed: 17512402]
28. Liu X, Gaubitz C, Pajak J, and Kelch BA (2022). A second DNA binding site on RFC facilitates clamp loading at gapped or nicked DNA. Elife 11, e77483. 10.7554/eLife.77483. [PubMed: 35731107]
29. Zheng F, Georgescu R, Yao NY, Li H, and O'Donnell ME (2022). Cryo-EM structures reveal that RFC recognizes both the 3'- and 5'-DNA ends to load PCNA onto gaps for DNA repair. Elife 11, e77469. 10.7554/eLife.77469. [PubMed: 35829698]
30. Schrecker M, Castaneda JC, Devbhandari S, Kumar C, Remus D, and Hite RK (2022). Multistep loading of a DNA sliding clamp onto DNA by replication factor C. Elife 11, e78253. 10.7554/eLife.78253. [PubMed: 35939393]
31. Li H, O'Donnell M, and Kelch B (2022). Unexpected new insights into DNA clamp loaders: Eukaryotic clamp loaders contain a second DNA site for recessed 5′ ends that facilitates repair and signals DNA damage: Eukaryotic clamp loaders contain a second DNA site for recessed 5′ ends that facilitates repair and signals DNA damage. Bioessays 44, e2200154. 10.1002/bies.202200154. [PubMed: 36116108]
32. Indiani C, and O'Donnell M (2006). The replication clamp-loading machine at work in the three domains of life. Nat. Rev. Mol. Cell Biol 7, 751–761. 10.1038/nrm2022. [PubMed: 16955075]
33. Kelch BA, Makino DL, O'Donnell M, and Kuriyan J (2012). Clamp loader ATPases and the evolution of DNA replication machinery. BMC Biol. 10, 34. 10.1186/1741-7007-10-34. [PubMed: 22520345]
34. Jeruzalmi D, O'Donnell M, and Kuriyan J (2001). Crystal structure of the processivity clamp loader gamma (gamma) complex of E. coli DNA polymerase III. Cell 106, 429–441. 10.1016/s0092-8674(01)00463-9. [PubMed: 11525729]
35. Bowman GD, O'Donnell M, and Kuriyan J (2004). Structural analysis of a eukaryotic sliding DNA clamp-clamp loader complex. Nature 429, 724–730. 10.1038/nature02585. [PubMed: 15201901]
36. Gaubitz C, Liu X, Magrino J, Stone NP, Landeck J, Hedglin M, and Kelch BA (2020). Structure of the human clamp loader reveals an autoinhibited conformation of a substrate-bound AAA+ switch. Proc. Natl. Acad. Sci. USA 117, 23571–23580. 10.1073/pnas.2007437117. [PubMed: 32907938]
37. Kelch BA (2016). Review: The lord of the rings: Structure and mechanism of the sliding clamp loader. Biopolymers 105, 532–546. 10.1002/bip.22827. [PubMed: 26918303]
38. Gaubitz C, Liu X, Pajak J, Stone NP, Hayes JA, Demo G, and Kelch BA (2022). Cryo-EM structures reveal high-resolution mechanism of a DNA polymerase sliding clamp loader. Elife 11, e74175. 10.7554/eLife.74175. [PubMed: 35179493]
39. Ellison V, and Stillman B (2003). Biochemical characterization of DNA damage checkpoint complexes: clamp loader and clamp complexes with specificity for 5' recessed DNA. PLoS Biol. 1, E33. 10.1371/journal.pbio.0000033. [PubMed: 14624239]
40. Majka J, and Burgers PMJ (2003). Yeast Rad17/Mec3/Ddc1: a sliding clamp for the DNA damage checkpoint. Proc. Natl. Acad. Sci. USA 100, 2249–2254. 10.1073/pnas.0437148100. [PubMed: 12604797]
41. Majka J, Binz SK, Wold MS, and Burgers PMJ (2006). Replication protein A directs loading of the DNA damage checkpoint clamp to 5'-DNA junctions. J. Biol. Chem 281, 27855–27861. 10.1074/jbc.M605176200. [PubMed: 16864589]
42. Castaneda JC, Schrecker M, Remus D, and Hite RK (2022). Mechanisms of loading and release of the 9-1-1 checkpoint clamp. Nat. Struct. Mol. Biol 29, 369–375. 10.1038/s41594-022-00741-7. [PubMed: 35314831]
43. Zheng F, Georgescu RE, Yao NY, O'Donnell ME, and Li H (2022). DNA is loaded through the 9-1-1 DNA checkpoint clamp in the opposite direction of the PCNA clamp. Nat. Struct. Mol. Biol 29, 376–385. 10.1038/s41594-022-00742-6. [PubMed: 35314830]
44. Day M, Oliver AW, and Pearl LH (2022). Structure of the human RAD17-RFC clamp loader and 9-1-1 checkpoint clamp bound to a dsDNA-ssDNA junction. Nucleic Acids Res. 50, 8279–8289. 10.1093/nar/gkac588. [PubMed: 35819203]
45. Sabbioneda S, Minesinger BK, Giannattasio M, Plevani P, Muzi-Falconi M, and Jinks-Robertson S (2005). The 9-1-1 checkpoint clamp physically interacts with polzeta and is partially required

for spontaneous polzeta-dependent mutagenesis in Saccharomyces cerevisiae. J. Biol. Chem 280, 38657–38665. 10.1074/jbc.M507638200. [PubMed: 16169844]

46. Toueille M, El-Andaloussi N, Frouin I, Freire R, Funk D, Shevelev I, Friedrich-Heineken E, Villani G, Hottiger MO, and Hübscher U (2004). The human Rad9/Rad1/Hus1 damage sensor clamp interacts with DNA polymerase beta and increases its DNA substrate utilisation efficiency: implications for DNA repair. Nucleic Acids Res. 32, 3316–3324. 10.1093/nar/gkh652. [PubMed: 15314187]
47. Schrecker M, Castaneda JC, Devbhandari S, Kumar C, Remus D, and Hite RK (2022). Multistep loading of PCNA onto DNA by RFC. Preprint at bioRxiv. 10.1101/2022.02.09.479782.
48. Bell SP, and Labib K (2016). Chromosome Duplication in Saccharomyces cerevisiae. Genetics 203, 1027–1067. 10.1534/genetics.115.186452. [PubMed: 27384026]
49. Stodola JL, and Burgers PM (2016). Resolving individual steps of Okazaki-fragment maturation at a millisecond timescale. Nat. Struct. Mol. Biol 23, 402–408. 10.1038/nsmb.3207. [PubMed: 27065195]
50. Punjani A, Rubinstein JL, Fleet DJ, and Brubaker MA (2017). cryo-SPARC: algorithms for rapid unsupervised cryo-EM structure determination. Nat. Methods 14, 290–296. 10.1038/nmeth.4169. [PubMed: 28165473]
51. Kimanius D, Dong L, Sharov G, Nakane T, and Scheres SHW (2021). New tools for automated cryo-EM single-particle analysis in RELION-4.0. Biochem. J 478, 4169–4185. 10.1042/BCJ20210708. [PubMed: 34783343]
52. Simonetta KR, Kazmirski SL, Goedken ER, Cantor AJ, Kelch BA, McNally R, Seyedin SN, Makino DL, O'Donnell M, and Kuriyan J (2009). The mechanism of ATP-dependent primer-template recognition by a clamp loader complex. Cell 137, 659–671. 10.1016/j.cell.2009.03.044. [PubMed: 19450514]
53. Chatterjee N, and Walker GC (2017). Mechanisms of DNA damage, repair, and mutagenesis. Environ. Mol. Mutagen 58, 235–263. 10.1002/em.22087. [PubMed: 28485537]
54. Yoo J, Lee D, Im H, Ji S, Oh S, Shin M, Park D, and Lee G (2021). The mechanism of gap creation by a multifunctional nuclease during base excision repair. Sci. Adv 7, eabg0076. 10.1126/sciadv.abg0076. [PubMed: 34261654]
55. Krokan HE, and Bjørås M (2013). Base excision repair. Cold Spring Harbor Perspect. Biol 5, a012583. 10.1101/cshperspect.a012583.
56. Acharya N, Prakash L, and Prakash S (2023). Yeast 9-1-1 complex acts as a sliding clamp for DNA synthesis by DNA polymerase ε. J. Biol. Chem 299, 102727. 10.1016/j.jbc.2022.102727. [PubMed: 36410434]
57. Yan S, and Michael WM (2009). TopBP1 and DNA polymerase-alpha directly recruit the 9-1-1 complex to stalled DNA replication forks. J. Cell Biol 184, 793–804. 10.1083/jcb.200810185. [PubMed: 19289795]
58. Kelman Z, Yao N, and O'Donnell M (1995). Escherichia coli expression vectors containing a protein kinase recognition motif, His6-tag and hemagglutinin epitope. Gene 166, 177–178. 10.1016/0378-1119(95)00556-7. [PubMed: 8529886]
59. Mastronarde DN (2003). SerialEM: A Program for Automated Tilt Series Acquisition on Tecnai Microscopes Using Prediction of Specimen Position. Microsc. Microanal 9, 1182–1183.
60. Scheres SHW (2012). RELION: implementation of a Bayesian approach to cryo-EM structure determination. J. Struct. Biol 180, 519–530. 10.1016/j.jsb.2012.09.006. [PubMed: 23000701]
61. Zheng SQ, Palovcak E, Armache JP, Verba KA, Cheng Y, and Agard DA (2017). MotionCor2: anisotropic correction of beam-induced motion for improved cryo-electron microscopy. Nat. Methods 14, 331–332. 10.1038/nmeth.4193. [PubMed: 28250466]
62. Rohou A, and Grigorieff N (2015). CTFFIND4: Fast and accurate defocus estimation from electron micrographs. J. Struct. Biol 192, 216–221. 10.1016/j.jsb.2015.08.008. [PubMed: 26278980]
63. Bepler T, Morin A, Rapp M, Brasch J, Shapiro L, Noble AJ, and Berger B (2019). Positive-unlabeled convolutional neural networks for particle picking in cryo-electron micrographs. Nat. Methods 16, 1153–1160. 10.1038/s41592-019-0575-8. [PubMed: 31591578]
64. Asarnow D, Palovcak E, and Cheng Y (2019). UCSF pyem v0. 5 Zenodo. 10.5281/zenodo3576630.

65. Pettersen EF, Goddard TD, Huang CC, Couch GS, Greenblatt DM, Meng EC, and Ferrin TE (2004). UCSF Chimera–a visualization system for exploratory research and analysis. J. Comput. Chem 25, 1605–1612. 10.1002/jcc.20084. [PubMed: 15264254]

66. Goddard TD, Huang CC, Meng EC, Pettersen EF, Couch GS, Morris JH, and Ferrin TE (2018). UCSF ChimeraX: Meeting modern challenges in visualization and analysis. Protein Sci. 27, 14–25. 10.1002/pro.3235. [PubMed: 28710774]

67. Emsley P, Lohkamp B, Scott WG, and Cowtan K (2010). Features and development of Coot. Acta Crystallogr. D Biol. Crystallogr 66, 486–501. 10.1107/S0907444910007493. [PubMed: 20383002]

68. Adams PD, Afonine PV, Bunkóczi G, Chen VB, Davis IW, Echols N, Headd JJ, Hung LW, Kapral GJ, Grosse-Kunstleve RW, et al. (2010). PHENIX: a comprehensive Python-based system for macromolecular structure solution. Acta Crystallogr. D Biol. Crystallogr 66, 213–221. 10.1107/S0907444909052925. [PubMed: 20124702]

69. Henricksen LA, Umbricht CB, and Wold MS (1994). Recombinant replication protein A: expression, complex formation, and functional characterization. J. Biol. Chem 269, 11121–11132. [PubMed: 8157639]

70. Zheng F, Georgescu RE, Li H, and O'Donnell ME (2020). Structure of eukaryotic DNA polymerase delta bound to the PCNA clamp while encircling DNA. Proc. Natl. Acad. Sci. USA 117, 30344–30353. 10.1073/pnas.2017637117. [PubMed: 33203675]

71. Su CC, Lyu M, Morgan CE, Bolla JR, Robinson CV, and Yu EW (2021). A 'Build and Retrieve' methodology to simultaneously solve cryo-EM structures of membrane proteins. Nat. Methods 18, 69–75. 10.1038/s41592-020-01021-2. [PubMed: 33408407]

72. Asarnow D, Palovcak E, and Cheng Y (2019). UCSF pyem v0. 5 Zenodo, 3576630. 10.5281/zenodo.3576630.

73. Chen VB, Arendall WB 3rd, Headd JJ, Keedy DA, Immormino RM, Kapral GJ, Murray LW, Richardson JS, and Richardson DC (2010). MolProbity: all-atom structure validation for macromolecular crystallography. Acta Crystallogr. D Biol. Crystallogr 66, 12–21. 10.1107/S0907444909042073. [PubMed: 20057044]

74. Pettersen EF, Goddard TD, Huang CC, Meng EC, Couch GS, Croll TI, Morris JH, and Ferrin TE (2021). UCSF ChimeraX: Structure visualization for researchers, educators, and developers. Protein Sci. 30, 70–82. 10.1002/pro.3943. [PubMed: 32881101]

Highlights

- Cryo-EM captures a multi-step DNA loading process of the 9-1-1 clamp by Rad24-RFC
- The 9-1-1 clamp is loaded onto the 3′ end of a 10-nt gapped DNA by Rad24-RFC
- Rad24-RFC contains physical barriers limiting the gap size (≥5 nt) for 9-1-1 loading
- The 9-1-1 loading onto a gapped DNA is more efficient than onto a 5′ recessed DNA

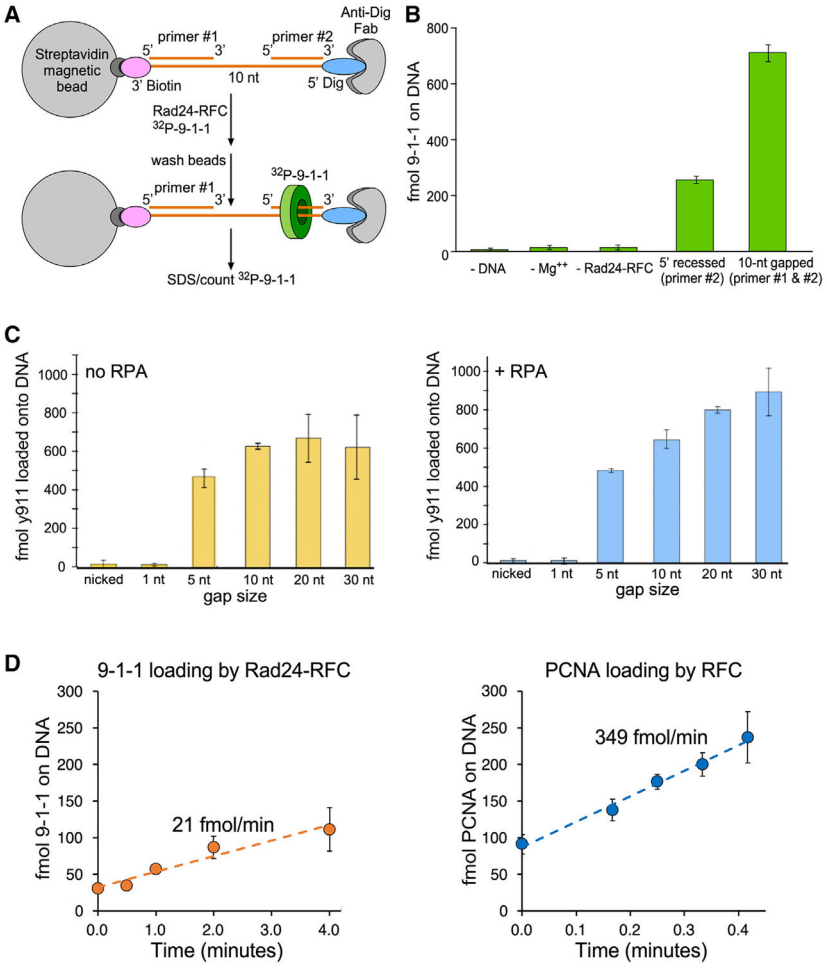

Figure 1. 9-1-1 loading onto gapped or 5′ recessed DNA substrates

(A) DNA oligos were annealed with a longer template DNA to provide either an isolated 5′ end (primer #2 only) or an ssDNA gap of various lengths (both primers #1 and #2; see Table S1). The ^{32}P-9-1-1 clamp is blocked from sliding by the biotin (attached to magnetic streptavidin beads) on one end and the DIG moiety attached to the Fab of an antibody to DIG at the other end. See STAR Methods for details.

(B) Comparison of 9-1-1 loading at a recessed 5′ end and at a 10-nt gap in the presence of RPA, along with control reactions lacking one assay component.

(C) Magnetic bead assays using nicked DNA or different-sized gaps either minus RPA (left) or plus RPA (right).

(D) Comparison of DNA loading rates of 9-1-1 (by Rad24-RFC) and PCNA (by RFC) were performed under identical conditions using the 10-nt gap DNA. Each experiment using the magnetic bead assay of (B)–(D) was carried out using three independently performed experiments. The data of are shown as standard error (SD) of the mean (SEM) performed by Microsoft Excel v.16.71.

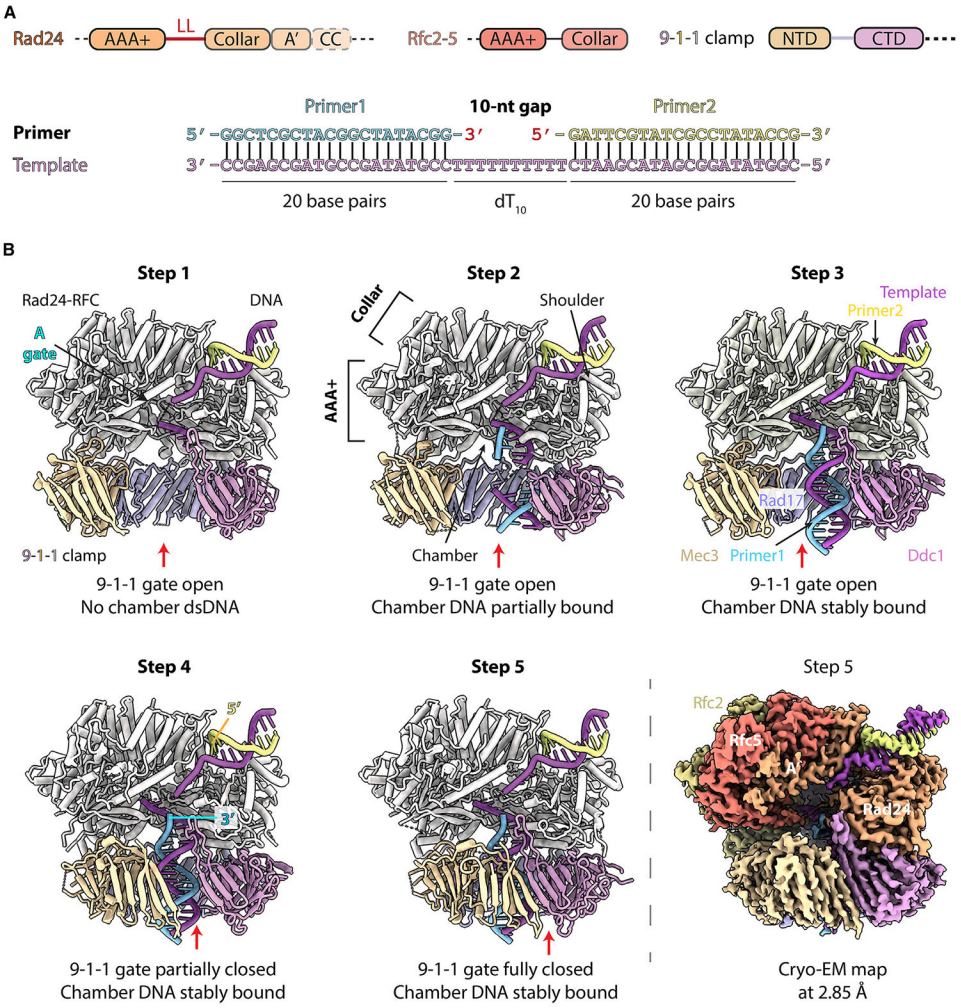

Figure 2. Five Rad24-RFC intermediates in loading 9-1-1 clamp onto a 10-nt gapped DNA

(A) Domain architecture of Rad24-RFC, 9-1-1 clamp, and the 10-nt gapped DNA. The Rfc2-5 and three subunits of 9-1-1 have similar respective domain arrangements and are shown together for brevity. Dashed lines indicate unsolved regions in EM maps. LL is the long linker between the Rad24 AAA+ module and the collar domain. The N-terminal domain (NTD) and CTD in each 9-1-1 subunit are linked by the inter-domain connecting loop (IDCL). The 10-nt gapped DNA harbors both 5′ and 3′ junctions.

(B) Structures of five Rad24-RFC loading intermediates of 9-1-1 clamp, arranged in a plausibly temporary sequence based on the progression of DNA binding in the central chamber of Rad24-RFC. In step 1, the 9-1-1 gate is open, and the DNA has not bound into the clamp loader chamber. In step 2, the 9-1-1 gate remains open, the DNA has entered the central chamber and passed through the 9-1-1-gate, but the DNA is partially stable, and the EM density for 4-bp DNA between the loader and the clamp is missing. In step 3, the 9-1-1 gate remains open, and the DNA in the chamber is fully stabilized. In step 4, the 9-1-1 gate is partially closed, and DNA is fully engaged. In step 5, the 9-1-1 gate is fully closed around the loaded DNA. A representative cryo-EM density map rendered at a high threshold (0.2) is shown at the bottom right corner. For clarity, the Rad24-RFC structure in all five models

is in ivory. The red arrow points to the 9-1-1 gate. The DNA entry A gate in Rad24-RFC is labeled in the step 1 structure. The structures are aligned and shown in the same front view.

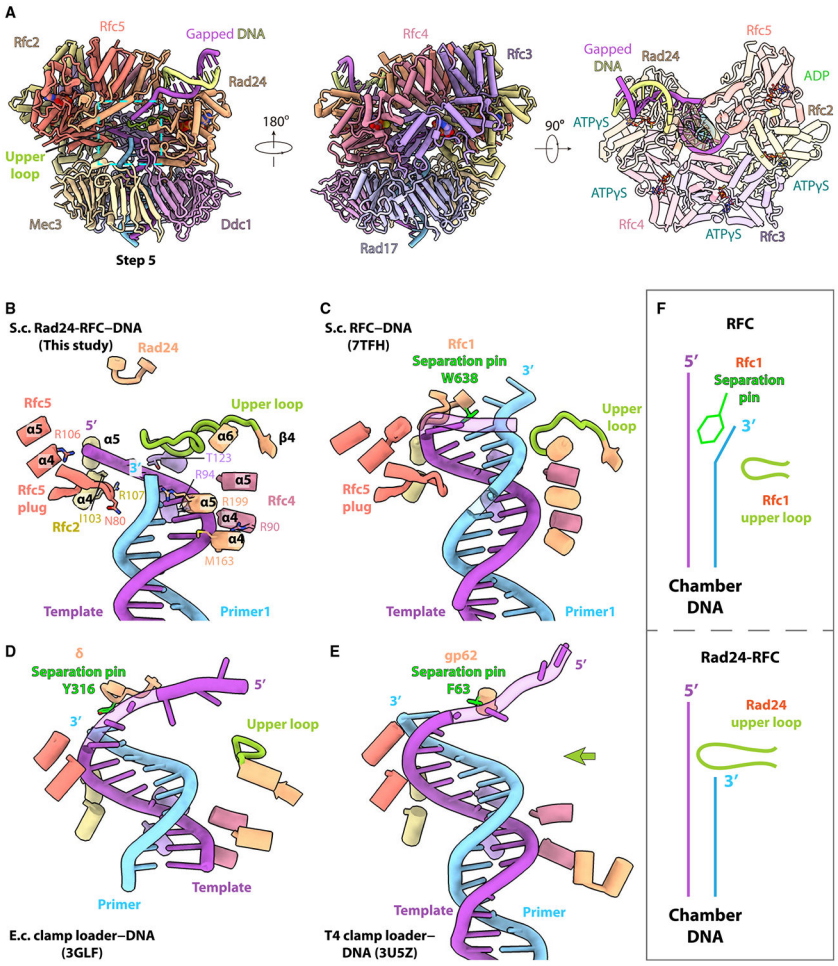

Figure 3. The Rad24 upper loop sets the gap size between the 3′ and 5′ DNA junctions

(A) The step 5 structure of Rad24-RFC–9-1-1–10-nt gapped DNA in a front (left), back (middle), and top (right) view. Subunits are individually colored. 9-1-1 is omitted in the right panel to better show the bound ATPγS and ADP. The Rad24 upper loop inside the chamber is highlighted in green. The region in the cyan box is shown enlarged in (B).

(B–F) Comparison of DNA binding in the chamber of Rad24-RFC (B), RFC (C), *E. coli* clamp loader (D), and T4 phage clamp loader (E). (F) Sketch comparing the 3′ DNA-binding mode in the chamber of RFC and Rad24-RFC based on structures in (B) and (C). The loaders are aligned but omitted except for a few labeled key elements. The α4 and α5 helices of each loader subunit follow and wrap around the template strand in purple. In (B), Rad24 Arg-199 and Rfc5 Asn-80 H-bond with the primer phosphate backbone in blue. The Rad24 upper loop blocks the primer strand from advancing upward, in contrast to the higher reach of the primers in all other loaders. The equivalent loops in other loaders are much shorter and do not block the primer strand (C and D). The T4 loader lacks the equivalent loop (indicated by a green arrow) as the corresponding AAA+ module is highly degenerated (E) (see also Figures S4B and S5). Notably, all clamp loaders—except for Rad24-RFC—harbor an aromatic residue (lime) at the top that functions as a separation pin to unwind DNA from the 3′ junction.

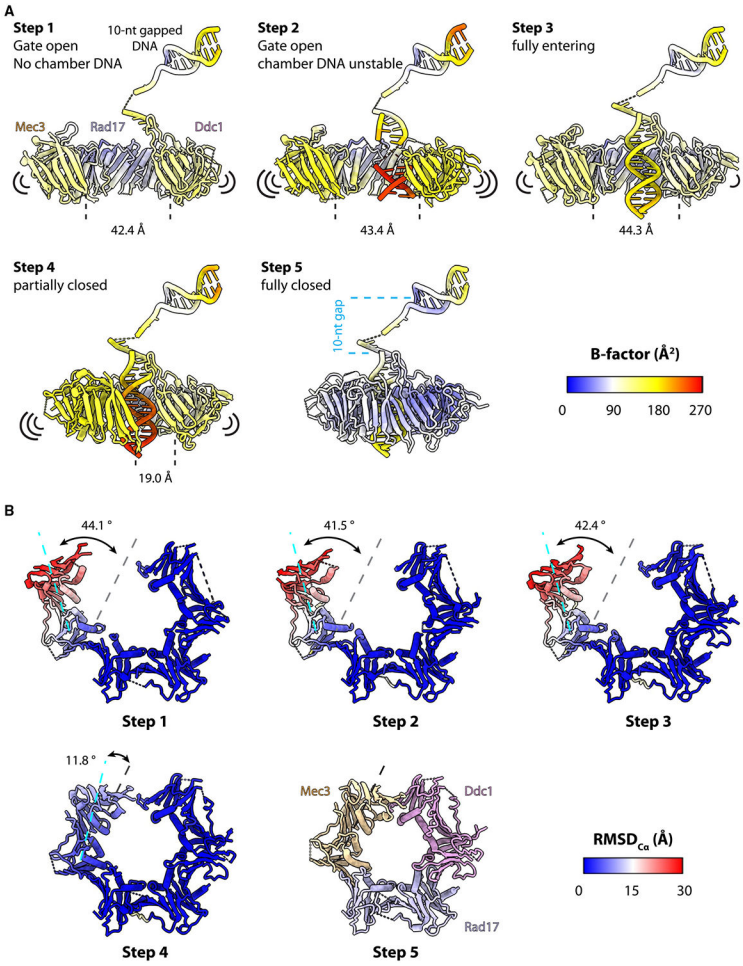

Figure 4. Gradual closure of the 9-1-1 gate accompanying DNA binding

(A) Flexibility analysis of the five loading intermediates. The atomic models are colored by their respective local B factors in ChimeraX. Rad24-RFC is omitted for clarity. Mec3 and Ddc1 lining the DNA gate are partially mobile (yellow) in the open gate and the partially open gate in steps 1–4, but they become stable (blue) in the closed gate in step 5. Consistent with the assigned temporal sequence, the chamber DNA is absent in step 1, is present but flexibly bound (red) in step 2, and becomes more stably bound (yellow) in step 3. The partial gate closure in step 4 destabilizes the chamber DNA (red), likely due to the perturbation by Mec3 movement. The chamber DNA is better stabilized in the 9-1-1 gate fully closed step 5. The 9-1-1 gate size is labeled. Four nucleotides and three nucleotides near the top 5′ junction and the bottom 3′ junction, respectively, are stabilized in the Rad24-RFC chamber. The dashed line represents three disordered nucleotides in the gap region. Because the Rad24-RFC A gate is open in all structures, ssDNA longer than 10 nt in the gap region can be easily accommodated by looping outward through the A gate.

(B) Although both Mec3 and Ddc1 line the DNA entry gate, Mec3 is the actual “gate” of the 9-1-1 clamp. The 9-1-1 structures in steps 1–4 are colored by their local $RMSD_{Cα}$ compared with the step 5 structure. Ddc1 is static, and gate opening and closing only involve the in-plane rotation of Mec3.

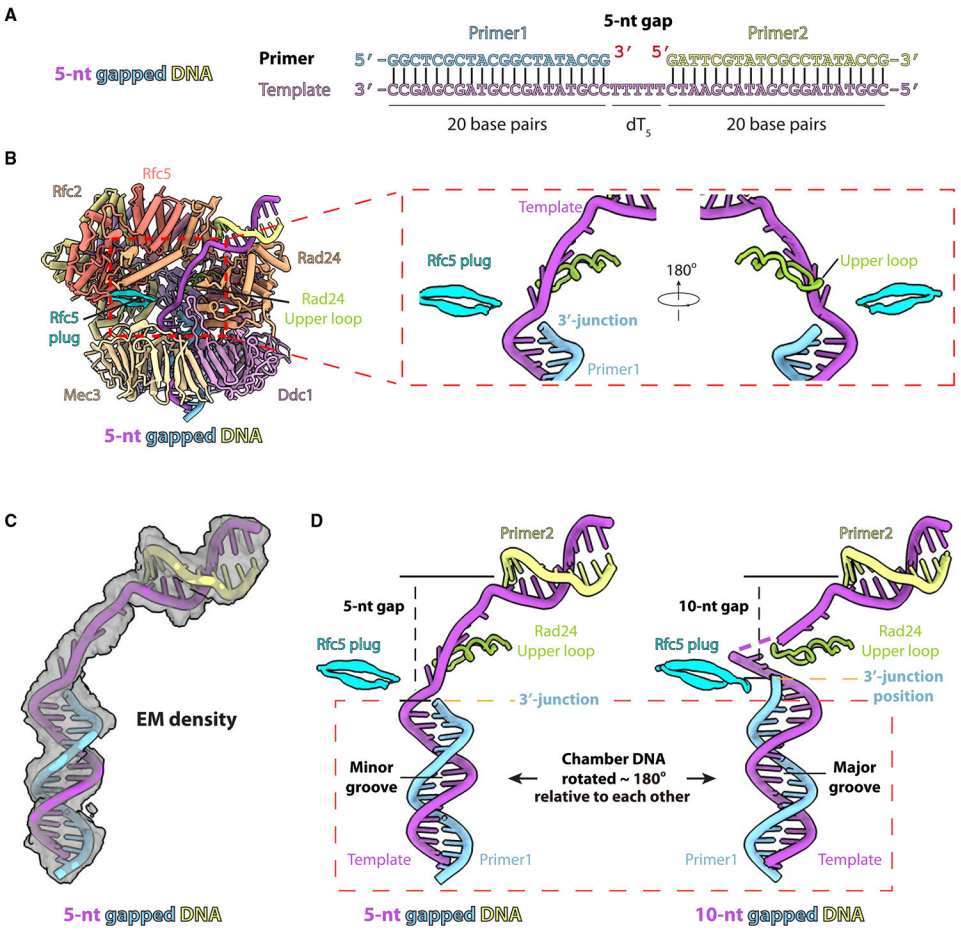

Figure 5. The Rad24 upper loop remains in place to block the advance of 3′ junction of the 5-nt gapped DNA

(A) A sketch of the used 5-nt gapped DNA substrate.

(B) Structure of the Rad24-RFC–9-1-1–5-nt gapped DNA complex in a front view. Subunits are individually colored. Right panel shows enlarged views of the 5-nt DNA gap region. The Rad24 upper loop and the Rfc5 plug are shown at the 3′ DNA junction to block the upward movement of the chamber DNA (i.e., DNA bound in the central chamber of Rad24-RFC).

(C) EM map of the 5-nt gapped DNA is shown in transparent gray surface and superimposed on the atomic model. The auto-refined map by Relion before post-processing at 3.66-Å resolution has stronger DNA density and is used here.

(D) Side-by-side comparison of the Rad24 upper loop (green) and Rfc5 plug (cyan) interacting with the 5-nt gapped DNA (left) and the 10-nt gapped DNA from step 5 (right). Note that the lower 3′ dsDNA in the left structure is rotated by 180° around its helical axis such that the purple template strand is oriented to connect with the upper 5′ dsDNA with a minimum length (5 nt).

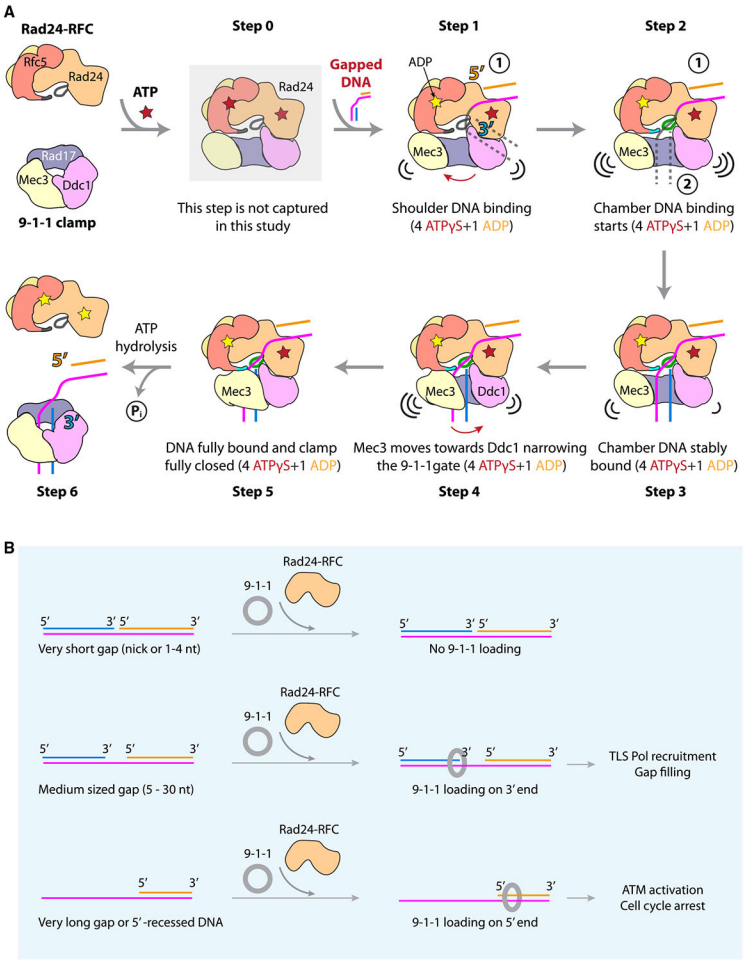

Figure 6. Proposed model of Rad24-RFC loading the 9-1-1 clamp onto a gapped DNA

(A) In preparation for loading (step 0), Rad24-RFC binds the 9-1-1 clamp to form a binary complex in the presence of ATP (or ATPγS used in this study). In a mechanism similar to the mutual activation of RFC and PCNA,[38] we suggest that binding energy between Rad24-RFC and 9-1-1 drives the DNA gate opening in Rad24-RFC (the A gate) and 9-1-1 (between Mec3 and Ddc1). This intermediate is grayed out as it is yet to be captured. In step 1, the shoulder DNA binds first to the Rad24-RFC external site. This is followed by the chamber DNA binding and passing through the 9-1-1 gate in steps 2 and 3. Once the DNA has fully entered, in steps 4 and 5, Mec3 moves toward Ddc1 to close the 9-1-1 gate, as indicated by the curved red arrow. The green Rad24 upper loop, with the help of the cyan Rfc5 plug, prevents DNA with a gap size shorter than 5 nt from entering the Rad24-RFC chamber. The consistent presence of four ATPγS and one ADP throughout steps 1 to 4 suggests that ATP hydrolysis is not required for DNA binding and clamp gate closure. Stable DNA binding and clamp gate closure likely induce a conformational change in Rad24-RFC to trigger ATP hydrolysis, leading to the dissociation of Rad24-RFC from 9-1-1 in step 6, leaving 9-1-1 alone encircling the DNA 3′ end.

(B) A sketch illustrating that Rad24-RFC does not load 9-1-1 onto a nicked DNA or very short gap (1–4 nt). By virtue of its recognition to the 5′ end, Rad24-RFC loads 9-1-1 to the 3′ end of a medium-sized gap, but loading at a very long gap or a 5′ recessed DNA leads

to loading onto ssDNA at a 5′ ssDNA junction, which is a very different outcome. Loading on the duplex of a 3′ end enables the 9-1-1 clamp to be used by a Pol, such as TLS Pol recruitment for gap filling at 3′ end, while loading at a 5′ end may result in ATM activation and cell-cycle arrest.

Table 1.

Cryo-EM data collection, refinement, and atomic model validation

	Rad24-RFC-9-1-1-10-nt gapped DNA					
Structures	**Step 1**	**Step 2**	**Step 3**	**Step 4**	**Step 5**	**5-nt gapped DNA bound**
EMDB ID	EMD-29412	EMD-29413	EMD-29414	EMD-29415	EMD-29416	EMD-29417
PDB ID	8FS3	8FS4	8FS5	8FS6	8FS7	8FS8
Data collection and processing						
Magnification	105,000					
Voltage (kV)	300					
Electron dose (e^{-}/Å^2)	64					
Under-focus range (μm)	1.3–1.9					
Pixel size (Å)	0.828					
Symmetry imposed	C1					
Initial particle images (no.)	3,256,498					5,857,353
Final particle images (no.)	255,777	347,098	400,932	191,448	292,725	242,906
Map resolution (Å)	2.93	2.94	2.76	2.90	2.85	3.04
FSC threshold	0.143					
Map resolution range (Å)	2.0–12.0	2.0–11.0	2.0–12.0	2.0–12.0	2.0–11.0	2.0–13.0
Refinement						
Initial model used (PDB code)	Step 5 model of this study				7SGZ, 7TFH	step 5
Map sharpening B factor (Å^2)	−86.9	−76.6	−82.6	−77.6	−82.0	−72.4
Map to model CC_{mask}	0.81	0.78	0.81	0.81	0.84	0.75
Model composition						
Non-hydrogen atoms	21,221	21,450	22,206	22,260	22,190	21,901
Protein and DNA residues	2,571; 27	2,538; 50	2,618; 58	2,623; 58	2,615; 58	2,581; 55
Ligands	9	9	9	9	9	9
RMSDs						
Bond lengths (Å)	0.004	0.004	0.003	0.003	0.003	0.002
Bond angels (°)	0.642	0.632	0.680	0.648	0.555	0.511
Validation						
MolProbity score	2.32	2.07	1.82	1.97	1.85	2.04

Structures	Rad24-RFC-9-1-1-10-nt gapped DNA					5-nt gapped DNA bound
	Step 1	Step 2	Step 3	Step 4	Step 5	
Clashscore	11.23	9.63	7.23	7.86	6.64	9.09
Poor rotamers (%)	4.18	2.65	1.73	2.53	2.28	3.17
Ramachandran plot						
Favored (%)	95.90	96.35	96.38	96.43	96.65	96.99
Allowed (%)	4.10	3.65	3.62	3.57	3.35	3.01
Disallowed (%)	0	0	0	0	0	0

KEY RESOURCES TABLE

REAGENT or RESOURCE	SOURCE	IDENTIFIER
Antibodies		
Anti-digoxigenin, fab fragments, sheep	Roche	Cat# 11214667001; RRID:AB_514494
Bacterial and virus strains		
E. coli DH5α competent cells	Thermo Fisher Scientific	Cat# 18265017
E. coli BL21(DE3) competent cells	Thermo Fisher Scientific	Cat# EC0114
Chemicals, peptides, and recombinant proteins		
[γ-^{32}P] ATP	PerkinElmer Life Sciences	Cat# BLU002Z500UC
ATPγS	Millipore Sigma	Cat# 11162306001
Bradford protein assay kit	Bio-Rad	Cat# 5000001
Dynabeads M-280 Streptavidin beads	Thermo Fisher Scientific	Cat# 11206D
Deposited data		
Cryo-EM map of Rad24-RFC–9-1-1 clamp–10-nt gapped DNA at step 1	This study	EMDB: EMD-29412
Cryo-EM map of Rad24-RFC–9-1-1 clamp–10-nt gapped DNA at step 2	This study	EMDB: EMD-29413
Cryo-EM map of Rad24-RFC–9-1-1 clamp–10-nt gapped DNA at step 3	This study	EMDB: EMD-29414
Cryo-EM map of Rad24-RFC–9-1-1 clamp–10-nt gapped DNA at step 4	This study	EMDB: EMD-29415
Cryo-EM map of Rad24-RFC–9-1-1 clamp–10-nt gapped DNA at step 5	This study	EMDB: EMD-29416
Cryo-EM map of Rad24-RFC–9-1-1 clamp–5-nt gapped DNA	This study	EMDB: EMD-29417
Atomic model of Rad24-RFC–9-1-1 clamp–10-nt gapped DNA at step 1	This study	PDB: 8FS3
Atomic model of Rad24-RFC–9-1-1 clamp–10-nt gapped DNA at step 2	This study	PDB: 8FS4
Atomic model of Rad24-RFC–9-1-1 clamp–10-nt gapped DNA at step 3	This study	PDB: 8FS5
Atomic model of Rad24-RFC–9-1-1 clamp–10-nt gapped DNA at step 4	This study	PDB: 8FS6
Atomic model of Rad24-RFC–9-1-1 clamp–10-nt gapped DNA at step 5	This study	PDB: 8FS7
Atomic model of Rad24-RFC–9-1-1 clamp–5-nt gapped DNA	This study	PDB: 8FS8
Oligonucleotides		
5′-TEG-Dig-CGGTATAGGCGATAC GAATCCC GTATAGCCGTAGCGA GCCCGACCATACC-3′ TEG-Biotin (isolated 5′ template)	Integrated DNA Technologies	N/A
5′-TEG-Dig-CGGTATAGGCGATAC GAATCTT TTTTTTTTCCGTATAGCCG TAGCGAGCCCGACCATACC-3′ TEG-Biotin (10-nt gapped template for loading assay)	Integrated DNA Technologies	N/A
5′-GGTATGGTCGGGCTCGCTACGG CTATA CGG-3′ (Primer 1 for loading assay)	Integrated DNA Technologies	N/A
5′-Phos-GATTCGTATCGCCTATACCG-3′ (Primer 2 for loading assay)	Integrated DNA Technologies	N/A
5′-CGGTATAGGCGATACGAAT CTTTTTTTTT TCCGTATAGCCG TAGCGAGCC-3′ (10-nt gapped template for EM grids making)	Integrated DNA Technologies	N/A
5′-CGGTATAGGCGATACGAATCTTT TTCCG TATAGCCGTAGCGAGCC-3′ (5-nt gapped template for EM grids making)	Integrated DNA Technologies	N/A
5′-GGCTCGCTACGGCTATACGG-3′ (Primer 1 for EM grids making)	Integrated DNA Technologies	N/A
5′-GATTCGTATCGCCTATACCG-3′ (Primer 2 for EM grids making)	Integrated DNA Technologies	N/A

REAGENT or RESOURCE	SOURCE	IDENTIFIER
Recombinant DNA		
cAMP-dependent protein kinase expression plasmid	Kelman et al.[58]	N/A
Rad24-RFC expression plasmid	Zheng et al.[43]	N/A
9-1-1 expression plasmid	Zheng et al.[43]	N/A
Software and algorithms		
SerialEM	Mastronarde[59]	https://bio3d.colorado.edu/SerialEM/
cryoSPARC v3.1.0 and v4.0.0	Punjani et al.[50]	https://cryosparc.com/
Relion 4.0	Scheres[60]	https://relion.readthedocs.io/en/release-4.0/
MotionCor2	Zheng et al.[61]	https://emcore.ucsf.edu/ucsf-software
CTFFIND4	Rohou and Grigorieff[62]	https://grigoriefflab.janelia.org/ctffind4
Topaz	Bepler et al.[63]	https://cb.csail.mit.edu/cb/topaz/
PyEM	Asarnow et al.[64]	https://zenodo.org/record/3576630#.ZDbbk-zMLsc
UCSF Chimera	Pettersen et al.[65]	http://www.cgl.ucsf.edu/chimera/
UCSF Chimera X	Goddard et al.[66]	https://www.cgl.ucsf.edu/chimerax/
Coot	Emsley et al.[67]	http://www2.mrc-lmb.cam.ac.uk/personal/pemsley/coot
PHENIX	Adams et al.[68]	https://phenix-online.org
Other		
Quantifoil Cu R2/1 300 mesh grids	SPI Supplies	Cat# 4330C-XA
Gatan Solarus plasma cleaner 950	Gatan	N/A
Vitrobot Mark IV	Thermo Fisher Scientific	N/A
Titan Krios G2 Cryo-TEM	Thermo Fisher Scientific	N/A